

**AN EVALUATION OF APOLLO
POWERED DESCENT GUIDANCE**

A Thesis
Presented to the
Faculty of
San Diego State University

In Partial Fulfillment
of the Requirements for the Degree
Master of Science in Aerospace Engineering
with a Concentration in
Guidance, Navigation, and Controls

by
Lloyd David Strohl III
Spring 2018

SAN DIEGO STATE UNIVERSITY

The Undersigned Faculty Committee Approves the
Thesis of Lloyd David Strohl III:

An Evaluation of Apollo
Powered Descent Guidance

Ping Lu, Chair
Department of Aerospace Engineering

Ahmad Bani Younes
Department of Aerospace Engineering

Peiman Naseradinmousavi
Department of Mechanical Engineering

Approval Date

Copyright © 2018
by
Lloyd David Strohl III

ABSTRACT OF THE THESIS

An Evaluation of Apollo
Powered Descent Guidance
by
Lloyd David Strohl III

Master of Science in Aerospace Engineering with a Concentration in Guidance,
Navigation, and Controls
San Diego State University, 2018

Powered descent guidance is a critical part of any aerospace mission with a heavy payload in sparse atmosphere or vacuum. It is also finding use in terrestrial landing for vehicle recovery. Powered descent presents the challenge of landing a vehicle softly while using as little fuel as possible. While much work has been done on powered descent guidance and fuel optimality, little consideration has been made of ignition timing and powered descent initiation. The powered descent phase is typically specified by a predetermined condition, altitude, or time. Adaptive Powered Descent Initiation (PDI) is proposed and tested as a strategy of initiating powered descent guidance automatically for robustness and improved propellant performance. Its effectiveness is tested by Monte Carlo simulation and results presented for a manned Mars mission. PDI is found to be especially effective in atmosphere as it extends the aerobraking phase without sacrificing safety and gaining propellant efficiency. Its closed-loop formulation ensures reliability in dispersed conditions reflective of practical mission conditions for Mars landing.

TABLE OF CONTENTS

	PAGE
ABSTRACT	iv
LIST OF TABLES.....	vii
LIST OF FIGURES	viii
ACKNOWLEDGMENTS	xi
 CHAPTER	
1 INTRODUCTION	1
1.1 Guidance and Control in Aerospace.....	1
1.2 Literature Review	2
1.3 Contribution	3
1.4 Organization	4
1.5 Problem Statement	5
2 METHODOLOGY.....	7
2.1 Notation.....	7
2.2 Coordinate Frame	9
2.3 Guidance Law	10
2.3.1 Equations of Motion.....	11
2.3.2 E-Guidance	12
2.3.3 Optimality.....	13
2.3.4 Apollo Powered Descent Guidance.....	15
2.3.5 Time-to-go	16
2.4 Adaptive Powered Descent Initiation	18
3 SIMULATION	21
3.1 Numerical Integration.....	22

3.2	Guidance Computer	23
3.3	Ignition trigger	24
3.4	Navigation Module.....	25
3.5	Aerodynamic Model	26
3.5.1	CobraMRV	26
3.5.2	Atmosphere Model	28
3.5.3	Orientation	28
3.6	Monte Carlo	29
3.7	Initial Condition	31
4	RESULTS	36
4.0.1	Adaptive PDI	37
4.0.2	Comparison of E-Guidance with APDG	38
4.0.3	Navigation Error	46
4.0.4	Vacuum vs. Atmosphere	51
4.0.5	Vacuum Performance	56
4.0.6	Atmospheric Performance.....	63
5	DISCUSSION	70
5.1	Simulation Error Analysis	70
5.2	Apollo Powered Descent Guidance	72
5.3	Adaptive Powered Descent Initiation	73
6	CONCLUSIONS AND FUTURE WORK	75
6.1	Adaptive Powered Descent Initiation	75
6.2	Future Work	75
	BIBLIOGRAPHY	79
	APPENDIX	
	DISPERSED TRAJECTORY FIGURES	81

LIST OF TABLES

	PAGE
3.1 Monte-Carlo Dispersion Settings.....	30
3.2 Initial Conditions for Mars Landing.....	31
4.1 Comparison of Performance of E-Guidance with APDG	43
4.2 Performance of APDG With and Without Navigation Error	47
4.3 Performance of APDG In Vacuum	60
4.4 Performance of APDG In Atmosphere.....	68

LIST OF FIGURES

	PAGE
2.1 Vehicle Body Axes. Source: Hall, N. Aircraft Rotations Body Axes. NASA Glenn Research Center, https://www.grc.nasa.gov/www/k-12/airplane/rotations.html , accessed February 2018	10
3.1 Simulation Architecture	21
3.2 CobraMRV Design. Source: C. Cerimele et al. A rigid mid lift-to-drag ratio approach to human mars entry, descent, and landing. AIAA Paper, 2017-1898, 2017.	27
3.3 Unpowered Initial Trajectory in Vacuum	32
3.4 Ground Range: Unpowered Initial Trajectory In Vacuum	33
3.5 Unpowered Initial Trajectory in Atmosphere	34
3.6 Unpowered Initial Trajectory in Atmosphere From Above	35
4.1 PDI Criteria: Vacuum	37
4.2 PDI Criteria: Atmopshere	38
4.3 Trajectory: E-Guidance vs. APDG	39
4.4 Altitude: E-Guidance vs. APDG	40
4.5 Ground Range: E-Guidance vs. APDG	40
4.6 Speed: E-Guidance vs. APDG	41
4.7 Thrust Magnitude: E-Guidance vs. APDG	41
4.8 Pitch: E-Guidance vs. APDG	42
4.9 Propellant Use Distribution: E-Guidance vs. APDG	44
4.10 Ground Range Distribution: E-Guidance vs. APDG	45
4.11 Speed Distribution: E-Guidance vs. APDG	46
4.12 Propellant Use Distribution: Nominal vs. Dispersed Navigation	49
4.13 Ground Range Distribution: Nominal vs. Dispersed Navigation	50

4.14	Speed Distribution: Nominal vs. Dispersed Navigation	51
4.15	Trajectory: Vacuum vs. Atmosphere	53
4.16	Altitude: Vacuum vs. Atmosphere	53
4.17	Ground Range: Vacuum vs. Atmosphere	54
4.18	Speed: Vacuum vs. Atmosphere	54
4.19	Thrust Magnitude: Vacuum vs. Atmosphere	55
4.20	Vehicle Mass: Vacuum vs. Atmosphere	55
4.21	Trajectory: APDG in Vacuum	57
4.22	Speed: APDG in Vacuum	57
4.23	Altitude: APDG in Vacuum	58
4.24	Ground Range: APDG in Vacuum	58
4.25	Thrust Magnitude: APDG in Vacuum	59
4.26	Case 1 Landing Sites: APDG in Vacuum	61
4.27	Fuel Histogram: APDG in Vacuum	62
4.28	Failures Histogram: APDG in Vacuum	63
4.29	Trajectory: APDG in Atmosphere	64
4.30	Altitude: APDG in Atmosphere	65
4.31	Ground Range: APDG in Atmosphere	65
4.32	Speed: APDG in Atmosphere	66
4.33	Thrust Magnitude: APDG in Atmosphere	66
4.34	Case 1 Landing Sites: APDG in Atmosphere	67
4.35	Fuel Histogram: APDG in Atmosphere	69
5.1	Convergence Test: Powered in Atmosphere	71
5.2	Convergence Test: Unpowered in Vacuum	72
6.1	PDI Time-to-go Factor: Thrust	77
6.2	PDI Time-to-go Factor: Speed	77
A.1	Ground Range Histogram: APDG in Vacuum	83

A.2	Speed Histogram: APDG in Vacuum	84
A.3	Ground Range Histogram: APDG in Atmosphere	85
A.4	Speed Histogram: APDG in Atmosphere	86
A.5	Failures Histogram: APDG in Atmosphere	87

ACKNOWLEDGMENTS

I would like to thank Dr. Lu for his serendipitous arrival at SDSU and consequent advice and instruction. With his mentoring and intuitive style, I have been able to launch an enjoyable and fulfilling career in GN&C, something I could not have achieved otherwise.

I would also like to thank Dr. Peter Blomgren both for his instruction and his work in developing and maintaining this thesis template.

CHAPTER 1

INTRODUCTION

A manned Mars mission places a heavy penalty on propellant inefficiency. This is because every kilogram of fuel required for landing must be delivered as payload through every phase of the mission until that point, and due to the exponential nature of Tsiolkovsky's rocket equation increasing landing payload mass is extremely expensive. The problem of powered descent guidance is then one of fuel optimality as well as safety, particularly in the case of a manned mission.

1.1 GUIDANCE AND CONTROL IN AEROSPACE

The powered descent guidance and soft landing problem under investigation is a problem requiring consideration of Guidance, Navigation, and Control principles and application.

Guidance refers to trajectory planning of a vehicle to satisfy mission conditions and constraints. For the soft landing problem, these conditions are the vehicle's initial state vector upon powered descent guidance initiation including its position and velocity, and the constraints are the desired final landing site, speed, and approach angle.

Navigation refers to the determination of the vehicle's state. For a manned Mars mission, the navigation systems available may be restricted to an internal inertial navigation system (INS), which numerically propagates an estimate of the vehicle's state based on measured accelerations. The vehicle may also have various other sensors which provide updates to its INS state estimate to improve accuracy. These sensors include radar, barometers, and the like.

Control refers to the manipulation of forces to induce the desired trajectory, orientation, or change of state. For the soft landing problem, these manipulations may be realized through aerodynamic surfaces, thrusters, rockets, or other systems which exert a force on the vehicle.

This paper seeks to investigate the trajectory planning aspect of powered descent guidance for soft landing in the context of a manned Mars mission. It does not examine Control or Navigation strategies in detail, though it does illustrate their importance.

1.2 LITERATURE REVIEW

The problem of powered descent guidance has been studied extensively throughout the last century, particularly since The Space Race of the 1960s and the Apollo program which spawned E-Guidance, presented first in Cherry [2]. These analyses have approached the problem in several different ways, but they generally share the requirement that the solution ensures soft landing in vacuum conditions. Most if not all of these analyses attempt to optimize fuel consumption due to the heavy penalty imposed on inefficient propellant use when landing on an extraterrestrial body. Almost all approaches also share the assumption of a fixed final time, computed or chosen in various ways. Few of them address the problem of powered descent initiation, or when to start powered descent guidance. None investigate powered descent initiation with E-Guidance in the context of a manned mission landing in atmosphere. Work has been done in mission phase planning but little optimization has been done for an initial trajectory with free ignition time.

Cherry developed E-Guidance, of which Apollo Powered Descent Guidance (APDG) is a version. APDG solves the Equations of Motion (2.11) and (2.12) by defining a linear or quadratic thrust acceleration profile which ensures satisfaction of the terminal constraints (2.13), (2.14), and (for constrained final attitude) (2.30). These two methods require choosing a fixed final time t_f , and Cherry proposes an algorithm similar to Algorithm (1). The final time t_f is dependent upon the initial conditions and assumes powered descent guidance is active. Other work has been done regarding the performance of APDG including landing site redesignation [18, 15] as well as robustness [8].

One well-studied powered descent solution is given by a gravity turn maneuver [11, 3, 4], which does not consider landing site redesignation but can be carefully initiated to achieve a predetermined landing site and ensures soft landing. Formulations of the gravity turn solution differ in application and approach, but typically the maneuver involves providing a thrust acceleration to exactly cancel the velocity vector upon

landing. This approach does not reliably satisfy the full powered descent guidance problem under study with designated landing sites and dispersed trajectories, but its analysis proves useful in determining a time-to-go and criteria for Adaptive Powered Descent Initiation.

D’Souza [5] did consider an optimal time-to-go, the remaining flight time at any given moment of the powered descent trajectory. D’Souza’s solution minimizes a weighted function of the time-to-go and the performance index given in Equation (2.20). As discussed below, minimizing this performance index is not fuel optimal but by minimizing the time-to-go a better performance can be realized, as demonstrated in D’Souza’s paper as well as several others [14, 17]. However, these approaches still only consider the problem after ignition, when the powered descent guidance phase has already begun.

Rea and Bishop [16] examined the fuel optimal powered descent guidance problem. They explored a time-to-go which optimizes their fuel optimal performance index, but it only considers the portion of flight after a deorbiting “braking” maneuver which ends when the vehicle altitude reaches some pre-designated altitude.

Meditch [12] showed that the fuel optimal thrust profile for a vertical landing given lower and upper thrust bounds is a “bang-bang” style thrust, where the thrust switches between its upper and lower bounds with at most one switch between the bounds during descent. The paper examined the one-dimensional fuel-optimal powered descent in a uniform gravitational field. This strategy may be directly applicable for the final touchdown phase, during which the E-Guidance solution must be stopped when time-to-go gets small as discussed in Section 3.2.

Leitmann [9] also examined a set of two-dimensional rocket flight problems including the two-dimensional powered descent and landing problem, similar to the problem under examination. Leitmann also showed that the fuel optimal thrust profile is “bang-bang,” with up to two switches.

1.3 CONTRIBUTION

This thesis seeks to improve upon APDG’s fuel performance in the context of a manned Mars mission. The unique aspects of this mission include high payload mass, the

aerodynamics of the landing vehicle, critical safety requirements, and the very high penalty for propellant inefficiency. The method by which APDG is improved is through adaptive powered descent initiation (PDI) which enhances fuel efficiency by making use of a longer glide slope during which energy is shed through lift and drag effects without thrust while delaying ignition to reduce burn time and more closely approximate the optimal thrust profile. The solution presented is equally as computationally expensive as traditional E-Guidance and does not rely on high rate thrust magnitude switching. The guidance law has been studied extensively and flown on real spacecraft.

The strategy of Adaptive PDI is applicable beyond the implementation of APDG. This strategy is valid for any multi-phase mission involving powered descent and could be employed in many other contexts. It has particular applicability for atmospheric landings due to the increased efficiency gained from aerodynamic effects, safely extending the glide and aerobraking phase.

1.4 ORGANIZATION

This thesis consists of a Methodology chapter in which equations are derived defining APDG and the Adaptive PDI strategy, a simulation chapter which details the simulation architecture and numerical implementation schemes used to test APDG and Adaptive PDI, a Results chapter in which the results of the simulation are presented, a Discussion chapter in which the results are examined and interpreted, and a Conclusions chapter in which conclusions are drawn from the results and future work is recommended on the topic of Adaptive PDI.

Chapter 1 introduces the soft landing problem and the motivation for Adaptive PDI. It defines the mission framework in which PDI is studied, and defines the powered descent guidance problem for derivation of APDG. It presents the relevant literature and prior work done on the topic of powered descent guidance and the contribution this thesis makes to that literature.

Chapter 2 derives E-Guidance and APDG, then presents the Adaptive PDI strategy and the relevant equations. It begins by defining the required notation and the coordinate frame used for the problem formulation.

Chapter 3 details the simulation architecture and numerical schemes used to implement Adaptive PDI with APDG and test its performance and robustness. The aerodynamic model is defined as well as the dispersion model for Monte Carlo testing. The initial conditions representing pre-determined Mars mission profile are given in Section 3.7.

Chapter 4 presents the results of simulation of the mission and makes several comparisons between various configurations. Section 4.0.1 investigates the reliability of the Adaptive PDI strategy and its applicability for a practical mission. Section 4.0.2 compares the performance of APDG with E-Guidance, since APDG is less well tested and no claims are made about its optimality. Section 4.0.3 investigates the effects of navigation error. Sections 4.0.4 through 4.0.6 presents results of simulation of a Mars mission and a similar mission in vacuum, comparing Adaptive PDI's performance to a traditional pre-determined ignition strategy.

Chapter 5 discusses the results of Chapter 4 and verifies the simulation output through error analysis.

Chapter 6 states the conclusions of the study and makes recommendations for future study of the Adaptive PDI strategy.

1.5 PROBLEM STATEMENT

Powered descent and landing is presented in the context of a manned Mars mission. This mission proceeds such that the powered descent guidance takes over after a successful de-orbiting and aerobraking maneuver when the vehicle is aerodynamically controllable (in a glide) near the landing site. The guidance algorithm for powered descent and soft landing is formulated under the following assumptions:

1. Atmospheric forces can be neglected
2. Rotation of the planetary body is accounted for by the terminal conditions and the guidance frame formulation
3. The vehicle's engine is not vectored such that the thrust is in line with the vehicle's yaw axis at all times
4. The vehicle's control system is perfect with zero lag
5. The nozzle exit velocity v_{ex} is a known constant

6. The thrust magnitude's upper bound is known
7. The vehicle's state can be reliably measured at all times, including measurement of local gravitational acceleration
8. The vehicle's thrust is throttleable between minimum and maximum values
9. Upon ignition, the vehicle can obtain commanded thrust within its upper and lower bounds instantaneously

Implicit in these assumptions is a specified landing condition which defines the guidance frame \hat{e} . It is desired to minimize propellant usage required by APDG through Adaptive PDI. It is essential that the solution is robust and reliable given the safety criticality of a manned mission. The last assumption is only relevant when ignition is started; APDG does not demand large instantaneous throttle responses. Taking into account ignition lag would be simple and not affect performance significantly, but it is not modeled here.

CHAPTER 2

METHODOLOGY

To investigate a guidance law with a careful focus on the time-to-go approach, a law must be developed and implemented in a simulation framework. The derivation of E-Guidance is presented here in the context of optimal control, as is the Adaptive Powered Descent Initiation (PDI) approach. The derivation of APDG is also presented without claim of optimality.

2.1 NOTATION

This paper uses a set of standard mathematical notation in deriving algorithms and describing models. That notation is defined here.

Vectors consisting of three coordinates in the guidance frame are indicated by boldface type as in Equation (2.1). Also relevant in this equation is that vectors are defined as column matrices.

$$\mathbf{V} = \begin{bmatrix} V_1 \\ V_2 \\ V_3 \end{bmatrix} \quad (2.1)$$

Matrices are represented by capital letters as in Equation (2.2). All matrices in this paper are 3x3 matrices.

$$A = \begin{bmatrix} a_1 & a_2 & a_3 \\ a_4 & a_5 & a_6 \\ a_7 & a_8 & a_9 \end{bmatrix} \quad (2.2)$$

A column vector \mathbf{V} may be converted to a row vector via a transpose operation.

$$\mathbf{V}^T = [V_1 \ V_2 \ V_3]$$

Vector multiplication arises mainly in three ways, all used throughout the guidance algorithm derivation. The first is the vector dot product, indicated as in Equation (2.3).

$$\mathbf{a} \cdot \mathbf{b} = \mathbf{a}^T \mathbf{b} = a_1 b_1 + a_2 b_2 + a_3 b_3 \quad (2.3)$$

Vectors consist of a magnitude and a direction. The magnitude is calculated by way of a vector norm operation as in Equation (2.4).

$$\|\mathbf{V}\| = \sqrt{\mathbf{V}^T \mathbf{V}} \quad (2.4)$$

The direction of a vector is itself a vector of magnitude 1 which points in the direction of the vector. A direction vector is indicated by a hat $\hat{\mathbf{g}}$ as in Equation (2.5). This equation represents the direction of gravitational acceleration as a function of position \mathbf{r} .

$$\hat{\mathbf{g}} = \frac{\mathbf{g}(\mathbf{r})}{\|\mathbf{g}(\mathbf{r})\|} \quad (2.5)$$

The second vector multiplication operation is the cross product of two vectors, indicated by \times as in Equation (2.6) for two vectors \mathbf{a} and \mathbf{b} in frame $\hat{\mathbf{e}}$, where $|A|$ represents the determinant of matrix A .

$$\mathbf{a} \times \mathbf{b} = \begin{vmatrix} \hat{\mathbf{e}}_1 & \hat{\mathbf{e}}_2 & \hat{\mathbf{e}}_3 \\ a_1 & a_2 & a_3 \\ b_1 & b_2 & b_3 \end{vmatrix} \quad (2.6)$$

The third vector multiplication operation is left matrix multiplication as in Equation (2.7). As shown, left matrix multiplication of a 3x3 matrix A with a 3x1 vector \mathbf{x} results in a 3x1 vector \mathbf{b} .

$$A\mathbf{x} = \mathbf{b} = \begin{bmatrix} b_1 \\ b_2 \\ b_3 \end{bmatrix} \quad (2.7)$$

Equation (2.7) can be interpreted as a system of linear equations in 3 unknowns: x_1 , x_2 , and x_3 . The solution to this linear system requires evaluation of the inverse of the matrix A , represented by A^{-1} .

Time derivatives are represented by dot notation as in Equation (2.8) showing the derivative relationship between position and velocity vectors.

$$\frac{d\mathbf{r}}{dt} = \dot{\mathbf{r}} = \mathbf{V} \quad (2.8)$$

2.2 COORDINATE FRAME

The guidance algorithm is developed within the guidance coordinate frame \hat{e} .

This frame can be defined in several ways. Cherry [2] used a gravitational body-centered frame to develop E-Guidance, but any inertial frame can be appropriate. The simulation uses a body-centered frame such that Initial and Final conditions are defined by longitudes, latitudes, and radii from the center of Mars. This simulation neglects the body rotation, but it could be taken into account by defining a rotated final landing site and would not alter the problem qualitatively. Gravitational acceleration is modeled as that of a spherical body, with radius of Mars $R_M = 3.396 * 10^6$. Equation (2.15) gives the vector equation for gravitational acceleration around a spherical body.

For convenience, these Initial Conditions are presented in Table 3.2 after a coordinate transformation to a frame centered on the landing cite so that the final position constraint (2.13) is at the origin. This frame is a right-handed system such that the first coordinate is Mars East, the second is Mars North, and the third is Mars up (the direction opposite the local gravitational acceleration, $-\hat{g}$). This E-N-U frame is intuitive because mission conditions such as ground range and altitude are directly represented.

The vehicle's aerodynamics depend upon its orientation, which can best be described in terms of its body axes as shown in Figure 2.1. This figure shows the classic definitions of body axes for Aerospace vehicles in atmosphere. The aircraft's orientation is described as a rotation of the body frame relative to the guidance frame. As depicted in the figure, the body frame of Equation 2.9 consists of the yaw, pitch, and roll body axes. Orientations are thus defined as rotations about the yaw axis, then the pitch axis, then the roll axis in a traditional Euler 3-2-1 sequence.

$$\hat{\mathbf{b}} = \begin{bmatrix} \hat{\mathbf{b}}_y \\ \hat{\mathbf{b}}_p \\ \hat{\mathbf{b}}_r \end{bmatrix} \quad (2.9)$$

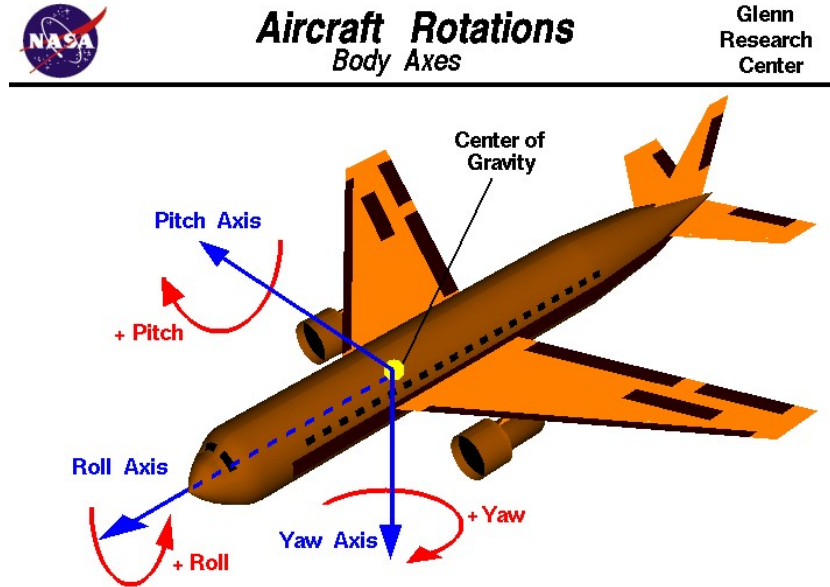


Figure 2.1. Vehicle Body Axes. Source: Hall, N. Aircraft Rotations Body Axes. NASA Glenn Research Center, <https://www.grc.nasa.gov/www/k-12/airplane/rotations.html>, accessed February 2018

2.3 GUIDANCE LAW

The guidance law under investigation is Apollo Powered Descent Guidance (APDG), first presented in Cherry [2]. APDG is a version of E-Guidance, which was developed empirically by integrating the equations of motion and choosing basis functions for the total acceleration \mathbf{a} that provided the necessary degrees of freedom to satisfy the terminal constraints in Equations (2.13) and (2.14). With control over thrust acceleration (and therefore total acceleration), satisfying the initial conditions after integration of the equations of motion requires two basis functions with vector coefficients. APDG extends this approach to a controlled final attitude by adding an additional constraint on final thrust acceleration $\mathbf{a}_{T_f}^*$ as in Equation (2.30), and satisfying these three vector constraints further requires a third basis function.

Guidance laws are typically presented as functions or systems defined over a range of time-to-go $t_{go} \in [t_{go_0}, 0]$. If the guidance command were recomputed without

updated state information in nominal conditions and with an extremely accurate physical model the vehicle would satisfy the terminal constraints without issue. However, in the presence of measurement error this open-loop strategy, which does not feed back the current state, will fail. Instead, these guidance laws can be recomputed at each update treating the current vehicle state as the initial condition for the guidance problem to be solved. In this way, the state feedback results in a closed-loop formulation that is robust and can much more accurately satisfy constraints in real-world applications. Good guidance law formulations result in arbitrary initial conditions such that the law can be implemented in a closed-loop fashion.

The derivation of E-Guidance as developed by Cherry proceeds below, followed by its formulation as an optimal guidance problem. APDG is then derived as developed by Cherry in a similar fashion though no claim is made about its optimality. The relative performance of the two laws is examined in Chapter 4.

2.3.1 Equations of Motion

Derivation of a powered descent guidance law begins with a formulation of the State Equation (2.10).

$$\dot{\mathbf{x}} = \mathbf{f}(\mathbf{x}, \mathbf{u}) \quad (2.10)$$

Cherry derives E-Guidance by treating this set of differential equations as a boundary value problem with initial conditions and final conditions to be satisfied by some command \mathbf{u} . Aerodynamic effects are not considered for development of the law, though they will be simulated and investigated with regards to performance.

The state equations for the 3-dimensional boundary value problem are as follows

$$\dot{\mathbf{r}} = \mathbf{V} \quad \mathbf{r}(t_0) = \mathbf{r}_0 \quad (2.11)$$

$$\dot{\mathbf{V}} = \mathbf{g}(\mathbf{r}) + \mathbf{a}_T \quad \mathbf{V}(t_0) = \mathbf{V}_0 \quad (2.12)$$

with terminal constraints at a fixed final time t_f

$$\mathbf{r}(t_f) = \mathbf{r}_f^* \quad (2.13)$$

$$\mathbf{V}(t_f) = \mathbf{V}_f^* \quad (2.14)$$

where \mathbf{a}_T is the thrust acceleration vector and $\mathbf{g}(\mathbf{r})$ is gravitational acceleration

$$\mathbf{g} = -\frac{\mu \mathbf{r}}{(\mathbf{r}^T \mathbf{r})^{(3/2)}} \quad (2.15)$$

where μ is the standard gravitational parameter for the body in question. For Mars, $\mu \approx 4.282 * 10^{13}$. Cherry recognized that the desired performance index for minimum propellant would minimize the integral of the thrust acceleration magnitude as in Equation (2.19). He also recognized that the thrust acceleration \mathbf{a}_T is limited such that

$$0 < a_{min} \leq \|\mathbf{a}_T\| \leq a_{max} \quad (2.16)$$

By choosing the command $\mathbf{u} = \mathbf{g}(\mathbf{r}) + \mathbf{a}_T$, the thrust acceleration command becomes $\mathbf{a}_T = \mathbf{u} - \mathbf{g}(\mathbf{r})$ so that the nonlinearities of the gravitational acceleration are effectively removed and a boundary value problem can be constructed by directly integrating the equations of motion and applying the boundary values to form a set of linear equations to be solved.

2.3.2 E-Guidance

While the set of non-linear equations presented in Section 2.3.1 do uniquely define a guidance command \mathbf{u} , Cherry recognized that they represented a “formidable bunch” of equations that he could not practically solve. Instead, he considered the infinite-dimensional generalized Fourier series that must represent the guidance command \mathbf{u} . By reducing the order of the Fourier series to equal the degrees of freedom demanded by the vector constraints of Equations (2.13) and (2.30), Cherry developed E-Guidance by considering first one guidance axis at a time, a “divide and conquer” strategy, so the x-component of the acceleration command took the form of Equation (2.17), where $\ddot{x} = a_x$, $p_1(t)$ and $p_2(t)$ are linearly independent functions of time, and c_1 and c_2 are unknown constants.

$$\ddot{x} = c_1 p_1(t) + c_2 p_2(t) \quad (2.17)$$

Cherry sets $p_1(t) = 1$ and $p_2(t) = t$, mostly for simplicity while recognizing that it may be suboptimal, arriving at a form identical to the one presented in Equation (2.22).

Cherry also proposes a time-to-go algorithm similar to that in Algorithm (1). It does not, however, do much to consider the optimality of this algorithm or, more critically, to deal with the problem of powered descent initiation.

2.3.3 Optimality

Cherry's solution for E-Guidance matches the solution to an optimal guidance problem with a particular performance index, though not precisely the fuel optimal index of Equation (2.19). The derivation of E-Guidance as an optimal guidance problem through the application of optimal control theory is presented here.

2.3.3.1 PERFORMANCE INDEX

Fuel consumption is related to the thrust acceleration vector by engine parameters represented by some positive constant k

$$\dot{m} = -k||\mathbf{a}_T|| \quad (2.18)$$

A fuel optimal guidance law should, therefore, use the performance index

$$J = \int_{t_0}^{t_f} ||\mathbf{a}_T|| dt \quad (2.19)$$

Choosing to minimize the square of the total acceleration $\mathbf{a} = \mathbf{g} + \mathbf{a}_T$ gives a performance index

$$J = \frac{1}{2} \int_{t_0}^{t_f} (\mathbf{g} + \mathbf{a}_T)^T (\mathbf{g} + \mathbf{a}_T) dt \quad (2.20)$$

For a constant gravitational acceleration \mathbf{g} , this performance index attempts to minimize $||\mathbf{a}_T||^2$. It is not fuel optimal as in Equation (2.19), but it does provide a cost to large thrust accelerations and might be expected to give good fuel performance.

2.3.3.2 E-GUIDANCE AS AN OPTIMAL GUIDANCE LAW

Choosing the guidance command $\mathbf{u} = \mathbf{g} + \mathbf{a}_T$ and applying optimal control theory results in the Hamiltonian in Equation (2.21) to be maximized and the steps following to define the behavior of the command \mathbf{u} .

$$H = \mathbf{p}_r^T \mathbf{V} + \mathbf{p}_V^T \mathbf{u} - \frac{1}{2} \mathbf{u}^T \mathbf{u} \quad (2.21)$$

$$\begin{aligned} \dot{\mathbf{p}}_r &= -\frac{\partial H}{\partial \mathbf{r}} = 0 \implies \mathbf{p}_r = -\mathbf{c}_2 \\ \dot{\mathbf{p}}_V &= -\frac{\partial H}{\partial \mathbf{V}} = -\mathbf{p}_r \implies \mathbf{p}_V = \mathbf{c}_1 + \mathbf{c}_2 t \\ \frac{\partial H}{\partial \mathbf{u}} &= 0 \implies \mathbf{u} = \mathbf{p}_V = \mathbf{c}_1 + \mathbf{c}_2 t \end{aligned}$$

For convenience, let $\tau = t_f - t$

$$\mathbf{u} = \mathbf{k}_1 + \mathbf{k}_2 \tau \quad (2.22)$$

where \mathbf{k}_1 and \mathbf{k}_2 are constant vectors.

Integrating the equations of motion with $\dot{\mathbf{V}} = \mathbf{u}$ then gives

$$\int \dot{\mathbf{V}}(t) dt = \mathbf{k}_1(t - t_0) + \frac{1}{2} \mathbf{k}_2(t - t_0)^2 + \mathbf{V}(t_0) \quad (2.23)$$

$$\int \dot{\mathbf{r}}(t) dt = \frac{1}{2} \mathbf{k}_1(t - t_0)^2 + \frac{1}{6} \mathbf{k}_2(t - t_0)^3 + \mathbf{V}(t_0)(t - t_0) + \mathbf{r}(t_0) \quad (2.24)$$

Setting $t = t_f$ and letting $t_{go} = t_f - t_0$ satisfies the terminal constraints from Equations (2.13) and (2.14), resulting in 6 linear equations in 6 unknowns

$$\mathbf{k}_1 t_{go} + \frac{1}{2} \mathbf{k}_2 t_{go}^2 = \mathbf{V}_f^* - \mathbf{V}_0 \quad (2.25)$$

$$\frac{1}{2} \mathbf{k}_1 t_{go}^2 + \frac{1}{6} \mathbf{k}_2 t_{go}^3 = \mathbf{r}_f^* - \mathbf{r}_0 - \mathbf{V}_0 t_{go} \quad (2.26)$$

These equations can be separated into sets of two per vector component. Define an inertial guidance frame $\hat{\mathbf{e}} = (\hat{x}, \hat{y}, \hat{z})^T$ such that guidance vector \mathbf{u} is composed of components in $\hat{\mathbf{e}}$, $\mathbf{u} = (u_x, u_y, u_z)^T$. For the equations in \hat{x} we have

$$\begin{bmatrix} t_{go} & \frac{1}{2}t_{go}^2 \\ \frac{1}{2}t_{go}^2 & \frac{1}{6}t_{go}^3 \end{bmatrix} \begin{pmatrix} k_{1x} \\ k_{2x} \end{pmatrix} = \begin{pmatrix} V_{fx}^* - V_{0x} \\ r_{fx}^* - (r_{0x} + V_{0x}t_{go}) \end{pmatrix} \quad (2.27)$$

Solving the two-equation system is accomplished by inverting the left-hand matrix, leading to a coefficient matrix E

$$E = \begin{bmatrix} -2/t_{go} & 6/t_{go}^2 \\ 6/t_{go}^2 & -12/t_{go}^3 \end{bmatrix} \quad (2.28)$$

The coefficients in \hat{x} are then

$$\begin{pmatrix} k_{1x} \\ k_{2x} \end{pmatrix} = E \begin{pmatrix} V_{fx}^* - V_{0x} \\ r_{fx}^* - (r_{0x} + V_{0x}t_{go}) \end{pmatrix} \quad (2.29)$$

It can be shown that the equations in \hat{y} and \hat{z} take the same form. This 2×2 E matrix is the origin of the name *E-Guidance*, the guidance law used in the Apollo lunar landing missions. Cherry formulated each version of E-Guidance, including APDG, by finding the inverted matrix E for the problem constraints.

2.3.4 Apollo Powered Descent Guidance

APDG enforces a final attitude constraint as a matter of practicality. A real rocket landing would typically require that the vehicle be oriented upright upon landing. Without explicitly enforcing a final attitude, the vehicle could touch down at a large angle while still satisfying final velocity and position constraints. For a vehicle whose attitude is determined by the thrust acceleration vector, this constraint can be implemented as a final thrust acceleration constraint as in Equation (2.30).

$$\mathbf{a}_T(t_f) = \mathbf{a}_{Tf}^* \quad (2.30)$$

A logical choice for this final thrust acceleration constraint is a vector in the negative gravitational acceleration direction as in Equation (2.31) where c is some positive scalar, ensuring that the vehicle touches down vertically.

$$\mathbf{a}_{T_f}^* = -c\hat{\mathbf{g}} \quad (2.31)$$

This vector constraint cannot be satisfied with only two basis functions for the command \mathbf{u} , so a third linearly independent function must be introduced such that $\mathbf{u} = \mathbf{c}_1 p_1(t) + \mathbf{c}_2 p_2(t) + \mathbf{c}_3 p_3(t)$. Cherry's choice for the third basis function is $p_3(t) = t^2$ for simplicity, with the other two functions the same as in E-Guidance.

After applying the substitution from Equation (2.22), this choice gives a command $\mathbf{u} = \mathbf{k}_1 + \mathbf{k}_2 \tau + \mathbf{k}_3 \tau^2$. This form for the command input is also easily integrable and leads to a similar linear system of 9 equations in \mathbf{k}_1 , \mathbf{k}_2 , and \mathbf{k}_3 . Using the same guidance frame $\hat{\mathbf{e}}$ defined for Equation (2.27) and considering one coordinate at a time we get a system similar to E-Guidance in Equation (2.32)

$$\begin{pmatrix} k_{1x} \\ k_{2x} \\ k_{3x} \end{pmatrix} = \begin{bmatrix} 0 & 0 & 1 \\ 18/t_{go}^2 & -24/t_{go}^3 & -6/t_{go} \\ -24/t_{go}^3 & 36/t_{go}^4 & 6/t_{go}^2 \end{bmatrix} \begin{pmatrix} V_{fx}^* - V_{0x} \\ r_{fx}^* - (r_{0x} + V_{0x}t_{go}) \\ g_x + a_{fx}^* \end{pmatrix} \quad (2.32)$$

2.3.5 Time-to-go

APDG depends upon a reliable estimate of remaining time-to-go (t_{go}). The E-Guidance formulation depends upon a fixed final time t_f , but does not explicitly constrain t_f since it is actually a free final-time problem. The Apollo mission's guidance used an estimate that updated continuously using Newton's method, but it was intended to only operate until initiation of the terminal descent phase at which point guidance switched to a manual vertical descent operation. Updating the t_{go} estimate continuously is attractive since it should be robust; if conditions have to change during the mission a closed-loop (continuously updating) solution will adjust and a new, realistic t_{go} will feed into the guidance solution. This quality was important to the Apollo Guidance solution because it relied upon pilot inputs to define the landing location visually, which meant allowing for landing site redesignations mid-mission. If t_{go} was not recomputed after site

redesignation, the guidance system would command unrealizable thrust acceleration commands. One closed-loop t_{go} algorithm is implemented in Algorithm (1).

Algorithm 1 Fixed-Point-Iteration t_{go}

```

1:  $tol \leftarrow c$ 
2: while  $|t_{go_0} - t_{go_1}| \geq tol$  do
3:    $t_{go_0} \leftarrow t_{go_1}$ 
4:    $\Delta V \leftarrow \sqrt{(\mathbf{V} - \mathbf{V}_0 + \mathbf{g} \cdot t_{go})^T (\mathbf{V} - \mathbf{V}_0 + \mathbf{g} \cdot t_{go})}$ 
5:    $t_{go_1} \leftarrow \frac{m_0}{\dot{m}} \left( e^{\frac{-\Delta V}{v_{ex}}} - 1 \right)$   $\triangleright \dot{m} < 0$ 
6: end while
7: return  $t_{go_1}$ 

```

Each guidance update uses the previous update's t_{go} minus clock time as its initial guess t_{go_0} , and the max iterations may be limited to some reasonable number. This algorithm requires an assumption about a fixed mass flow rate \dot{m} which is not guaranteed by the guidance law. Adjustment of this mass flow rate estimate is very particular to the initial conditions of the mission, resulting in a necessarily conservative t_{go} to account for initial condition dispersion.

For the purposes of this study, live landing site redesignation is not considered. Without the possibility of landing site redesignation, an open-loop t_{go} solution lends the guidance law more stability in that the performance is less dependent upon specific assumptions and conditions imposed by the t_{go} algorithm. One attractive open-loop option is the time to perform a gravity turn landing at maximum thrust. Equation (2.33) for a gravity turn time-to-go, $t_{go_{GT}}$, was presented in Citron, Dunin, and Meissinger [4]. Here, γ is flight path angle and R_M is the radius of Mars. After engine ignition and initiation of Powered Descent Guidance, the updated time-to-go is computed as $t_{go_{GT}}$ minus elapsed clock time. The algorithm for time-to-go using a gravity turn maneuver is given in Equation (2.33), where a_{GT} is the thrust acceleration magnitude applied during the maneuver. This equation gives two roots for a_{GT} , a positive root and a negative root. The desired root is positive (because this thrust acceleration magnitude), making it a simple matter to find. This quantity will be important in Section 2.4.

$$\begin{aligned}
\gamma &= \frac{\pi}{2} - \cos^{-1} \left(\frac{\mathbf{r}^T \mathbf{V}}{\|\mathbf{r}\| \|\mathbf{V}\|} \right) \\
g_m &= \|\mathbf{g}\| \\
r_m &= \|\mathbf{r}\| \\
V_m &= \|\mathbf{V}\| \\
a &= 1/g_m^2 \\
b &= \frac{\sin(\gamma) V_m^2}{2(r_m - R_M) g_m^2} \\
c &= -\frac{V_m^2 (1 + \sin(\gamma)^2)}{4(r_m - R_M) g_m} + 1 \\
a_{GT} &= \frac{-b \pm \sqrt{b^2 - 4ac}}{2a} \\
t_{go_{GT}} &= \frac{V_m}{2} \left(\frac{1 + \sin(\gamma)}{a_{GT} + g_m} + \frac{1 - \sin(\gamma)}{a_{GT} - g_m} \right)
\end{aligned} \tag{2.33}$$

A gravity turn landing does not directly apply to the powered descent guidance problem under investigation because it does not seek to satisfy the constraints given in Equations (2.13) and (2.14). However, if the magnitude of the terminal velocity target in Equation (2.14) is small, the required time to decelerate from an initial \mathbf{V}_0 under only the forces of thrust acceleration \mathbf{a}_T and gravity \mathbf{g} is, at minimum, the gravity turn solution $t_{go_{GT}}$. Since the terminal position \mathbf{r}_f is specified, the vehicle necessarily needs more time than given by the gravity turn solution to satisfy it. Assuming a small trajectory error requiring a small diversion to the landing site, a small constant factor $c_t \approx 1.2$ can be applied to the gravity turn time-to-go to allow for redirection. The choice of $c_t = 1.2$ proves to be sufficiently conservative to survive initial condition dispersion, rocket parameter dispersion, and navigation error in vacuum but unnecessary in atmosphere, where no correction factor is applied.

2.4 ADAPTIVE POWERED DESCENT INITIATION

The central focus of this thesis is the use of Adaptive Powered Descent Initiation (PDI) to improve the fuel performance and safety of APDG. This is accomplished by choosing an ignition time which results in superior propellant consumption while still

allowing soft landing. From Leitmann's [9] and Meditch's [12] work in one and two dimensions it is expected that a "bang-bang" style thrust profile is desirable. Lu 2017 [10] shows that for the three-dimensional problem the propellant optimal thrust profile is indeed "bang-bang" style and may have up to two switches. He also shows that the profile is further constrained to a final thrust value $T(t_f) = T_{max}$ in order to satisfy the final position and velocity constraints. With APDG controlling the thrust acceleration vector \mathbf{a}_T , a "bang-bang" style thrust profile will not be realized due to the continuous nature of the boundary-value problem presented, but the ignition time may be chosen to force a thrust profile closer to optimum. By choosing a time-to-go carefully, nearly optimal fuel performance may be expected.

Since APDG does not take the thrust acceleration limits of Equation (2.16) into account directly the time-to-go must do so or risk the required thrust acceleration exceeding the capabilities of the landing vehicle. One approach is to make use of the gravity turn solution Equation (2.33) as discussed in Section 2.3.5. This equation provides one criterion for ignition through the specified thrust acceleration \mathbf{a}_{GT} as in Algorithm (2). If the gravity turn time-to-go $t_{go_{GT}}$ is used and the engine ignited for APDG the moment the magnitude of the specified thrust acceleration a_{GT} reaches or exceeds the known maximum thrust acceleration magnitude a_{max} , APDG will command a large initial thrust acceleration which may exceed the rocket's limits and the thrust will be nearly or completely saturated at its upper limit. This approaches the optimal "bang-bang" style thrust profile using minimum thrust ($T = 0$) until ignition and nearly maximum thrust after ignition until landing. Using a padded $t_{go_{GT}}$ helps ensure that there is some margin for error.

Algorithm 2 Thrust Acceleration Criterion

- 1: **if** $|\mathbf{a}_{GT}| \geq \frac{T_{max}}{m}$ **then**
- 2: *ignite engine*
- 3: **end if**

Another important criterion is the downrange travel required by a gravity turn maneuver. The powered descent phase should be initiated if the horizontal distance

remaining in the velocity direction to the landing site is greater than or equal to the downrange distance traveled during a gravity turn maneuver. This will help ensure that the vehicle does not overshoot the landing site which would ultimately require far more fuel than necessary. Equation (2.34) gives the downrange distance traveled during a gravity turn maneuver s_{GT} , where h is the current altitude. Algorithm (3) details this ignition logic.

$$s_{GT} = \frac{V_m^2}{2a_{GT}} \cos(\gamma) \frac{V_m^2 + 2g_m h}{V_m^2 + g_m h} \frac{R_M}{r_m} \quad (2.34)$$

Algorithm 3 Range Criterion

```

1: if  $|s_{GT}| \leq |\mathbf{r}_{xy} - \mathbf{r}_{f_{xy}}|$  then
2:   ignite engine
3: end if

```

Notably, Cerimele et. al [1] recognize in the design of the CobraMRV (described in Section 3.5.1) that “the selection of the altitude to transition to powered descent ... is a crucial performance variable.” They suggest a timing strategy similar to that described in this section.

CHAPTER 3

SIMULATION

The powered descent simulation (PD Sim) is developed using standard programming techniques and numerical methods. The code is modular to facilitate design and reflect the functions of a mission computer. The simulation has three degrees of freedom (3-DoF) with derived orientation for force modeling. The simulation takes a set of initial conditions r_0 and V_0 , a set of final conditions r_f and V_f , dispersed rocket parameters, and nominal rocket parameters for the guidance module to use in its calculations of throttle setting. The overall simulation architecture is shown in Figure 3.1.

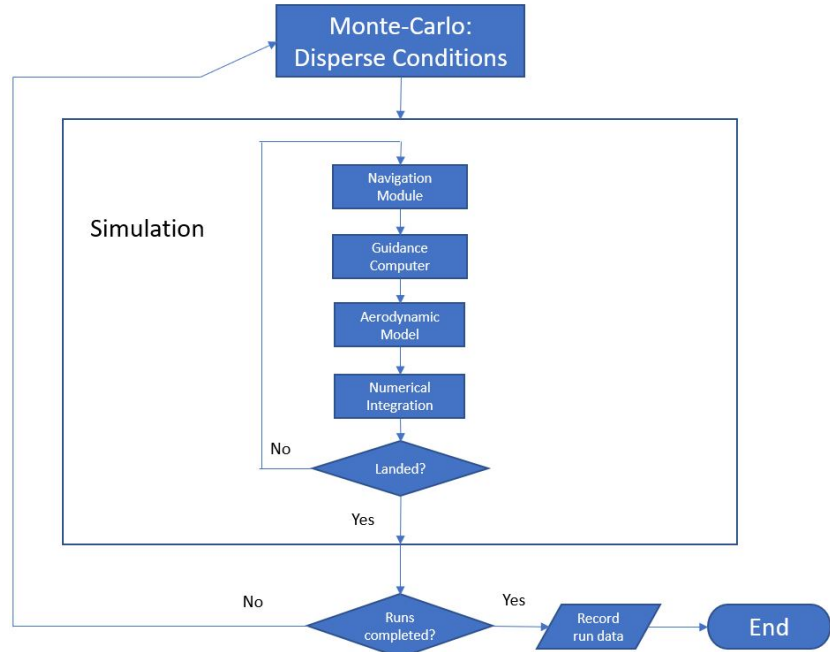


Figure 3.1. Simulation Architecture

At the core of the simulation is numerical time integration. The method employed is a 4th order Runge-Kutta (RK4). The RK4 function is called at each time step to progress the simulation forward.

The separate modules called during simulation are the guidance computer which contains the guidance law and computes a commanded thrust acceleration vector, the navigation module which generates a state estimate from simulated instrument measurements for use by the guidance computer, and the aerodynamic module which contains a model of the landing vehicle to compute forces and orientation for use in integration.

The simulation stops when either the vehicle passes through zero altitude (crashes) or the time-to-go is less than a single time integration step. When the latter condition is met, the time integration step is reduced to the remaining time-to-go and one more iteration is performed.

The full simulation code is wrapped in a Monte-Carlo script. The Monte-Carlo script calls the PD Sim with simulation settings, vehicle parameters, initial condition, and navigation uncertainty. This allows each individual run to have dispersed conditions without modification of the code.

Further detail for each part of the simulation follows.

3.1 NUMERICAL INTEGRATION

The numerical time integration is done via a standard Runge-Kutta formulation, presented here as in Ferziger and Perić 2002 [6]. The state vector ϕ is passed to the equations of motion $f(\phi, t)$ several times as in Equation (3.1). Δt , the time integration step for the simulation, is fixed at 1 millisecond (10^{-3} s). This is shown to be sufficiently small in Section 5.1.

$$\begin{aligned}
\phi_{n+\frac{1}{2}}^* &= \phi_n + \frac{\Delta t}{2} \mathbf{f}(t_n, \phi_n) \\
\phi_{n+\frac{1}{2}}^{**} &= \phi^n + \frac{\Delta t}{2} \mathbf{f}(t_{n+\frac{1}{2}}, \phi_{n+\frac{1}{2}}^*) \\
\phi_{n+1}^* &= \phi^n + \Delta t \mathbf{f}(t_{n+\frac{1}{2}}, \phi_{n+\frac{1}{2}}^{**}) \\
\phi_{n+1} &= \phi^n + \frac{\Delta t}{6} [\mathbf{f}(t_n, \phi_n) + 2\mathbf{f}(t_{n+\frac{1}{2}}, \phi_{n+\frac{1}{2}}^*) \\
&\quad + 2\mathbf{f}(t_{n+\frac{1}{2}}, \phi_{n+\frac{1}{2}}^{**}) + \mathbf{f}(t_{n+1}, \phi_{n+1}^*)]
\end{aligned} \tag{3.1}$$

The EOM function computes the derivative of the state vector ϕ . It is the same as the modeled equations of motion in Equations (2.11) and (2.12) but with an additional force term, \mathbf{F}_{LD} , to represent the vector sum of the aerodynamic forces of Lift and Drag, defined in Section 3.5.2. ϕ is passed in as a 6x1 column vector such that $\phi = [\mathbf{r}^T, \mathbf{V}^T]^T$, and the derivatives are calculated as in Equations (3.2) and (3.3).

$$\dot{\mathbf{r}} = \mathbf{V} \tag{3.2}$$

$$\dot{\mathbf{V}} = \mathbf{g}(\mathbf{r}) + \mathbf{a}_T + \frac{\mathbf{F}_{LD}}{m} \tag{3.3}$$

For simplicity, the vehicle's thrust acceleration response to a guidance command is modeled as zero-lag, i.e. perfect control. It assumes that the vehicle instantly and perfectly responds to the commanded \mathbf{a}_T , so the command from the guidance computer, after being put through a thrust magnitude limiter, is the same as the term in Equation (3.3). This is done to separate the study of Guidance laws from the performance of Control laws, as discussed in Section 1.1.

3.2 GUIDANCE COMPUTER

The guidance computer takes as input the current state as provided by the navigation system, the terminal constraints (final position and velocity in the case of E-Guidance, with final acceleration as well in the case of APDG), nominal vehicle max thrust, current vehicle mass, time-to-go, and selection of guidance law.

The output is a throttle setting as a fraction of the nominal max thrust and a direction for the thrust acceleration \mathbf{a}_T . These values are unlimited at the level of the

guidance computer, i.e. the throttle setting can be larger than 1 commanding thrust magnitude greater than T_{max} .

In this implementation, the throttle is limited after being passed out of the guidance computer to reflect the real performance constraint represented by Equation (2.16). Since the guidance computer only receives nominal T_{max} upon which to base its throttle setting, the resultant command can be off due to engine performance dispersion.

The guidance command is updated periodically at a rate lower than the simulation rate. Here the guidance is refreshed at 5 Hz. It must also stop updating when t_{go} becomes small due to its presence in the denominator for several entries in the E matrices of Equations (2.27) and (2.32). For the last half second the thrust acceleration is held constant. This has very little impact on landing precision as demonstrated in the Results chapter, Section 4.0.3.

The time-to-go computation takes place in the guidance module. The computation method is as described in Section 2.3.5. A gravity turn estimate is used to initialize the simulation, but it is reset upon ignition based on the current conditions and then allowed to run open-loop until simulation stop. The safety factor applied depends upon conditions. In vacuum, a constant factor $c_t = 1.2$ is necessarily applied to ensure soft landing when using the ignition optimization strategy. With atmospheric conditions the additional factor is unnecessary as is demonstrated in Section 4.0.6.

The guidance solution requires specification of the terminal constraints. In both E-Guidance and APDG, the terminal constraints for position and velocity are specified in the same frame as the initial conditions. For the initial conditions listed in Table 3.2, the final position constraint is the origin. The simulation operates in a Mars-centered frame in order to simplify gravitational calculations and model a spherical body easily, so the final position constraint seen by the guidance computer is $\mathbf{r}_f = [0, 0, R_M]^T$, where R_M is the radius of Mars. The final velocity is chosen as 1 m/s in the down direction. For APDG the final thrust acceleration is given as Equation (2.31), where c is chosen to be 2. This more strongly enforces the final attitude constraint than a smaller scalar without imposing too strong a requirement to the detriment of propellant performance.

3.3 IGNITION TRIGGER

Ignition time is determined by checking the two criterion discussed in Section 2.4: required thrust acceleration magnitude a_{GT} and downrange distanced traveled by a gravity turn maneuver s_{GT} . The vehicle is started in atmosphere on a trajectory roughly in line with the landing site as shown in Figures 3.4 and 3.6. As the vehicle travels along this trajectory with its engine off, these two criteria are constantly checked. Once either one is satisfied, the engine is ignited and the time-to-go estimate is updated as described in Section 3.2. Implementation of the ignition switch is performed in the simulation script by a simple flag that is checked upon guidance updates.

It is important to be certain that the criteria are met at some point in the flight. This strategy ensures that the ignition trigger is flipped in time as is discussed in Section 4.0.1. Figures 4.1 and 4.2 show that gravity turn required thrust acceleration magnitude monotonically increases throughout the unpowered trajectory, and downrange distance traveled in a gravity turn maneuver decreases faster than the vehicle's range from the landing site.

3.4 NAVIGATION MODULE

The navigation module is fairly simplistic. It has two functions.

The first function is to model navigation error in the form of normally distributed noise. The function takes the actual vehicle state \mathbf{r} and \mathbf{V} , adds noise with a distribution specified in the simulation settings of the Monte Carlo script, and creates \mathbf{r}_{nav} and \mathbf{V}_{nav} vectors. The noise distribution is chosen to reflect realistic navigation error as provided by an inertial navigation system per the trade study presented in Moesser 2010 [13].

Typical standard deviations are 1 m position error and 1/3 m/s velocity error.

The second function is to filter the noisy navigation measurements to produce a smoother estimate of the vehicle's state. It does this using a simple low-pass filter as in Equation (3.4), where α is a chosen filter constant (here $\alpha = 0.3$), \mathbf{x} is the current nav output of state, \mathbf{x}_{prev} is the previous filtered state estimate, and \mathbf{x}_{est} is the current filtered state estimate.

$$\mathbf{x}_{est} = \alpha \mathbf{x}_{prev} + (1 - \alpha) \mathbf{x} \quad (3.4)$$

A Kalman filter would likely be used on a more sophisticated navigation system for a real aerospace vehicle, but given the simplicity of the navigation error and perfect knowledge of the noise distribution, modeling a Kalman filter would likely provide too good an estimate effectively canceling the effects of the simulated navigation error.

3.5 AERODYNAMIC MODEL

The Aerodynamic model is comprised of Mars atmosphere data from NASA's Mars-GRAM 2010 [7], and the vehicle model was developed by Cerimele et. al [1]

3.5.1 CobraMRV

The vehicle model is taken from the CobraMRV design by Cerimele et. al [1]. The CobraMRV is a “rigid, enclosed, elongated lifting body shape that provides a higher lift-to-drag ratio (L/D) than a typical entry capsule...”. It was designed as an atmospheric entry and powered descent and landing vehicle for manned Mars missions compatible with the current NASA Human Mars mission architectures. These missions require delivery of roughly 20 tonnes of cargo to the surface. This vehicle, rendered in Figure 3.2 taken from Cerimele et. al, is designed such that its thrust vector is fixed in the direction of the body yaw axis, i.e. its thrust is oriented down when it is flying horizontally relative to the surface.

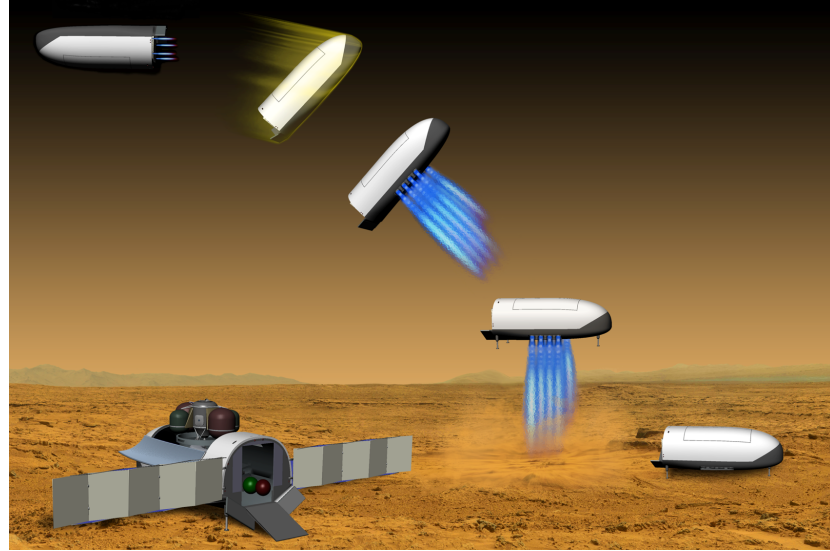


Figure 3.2. CobraMRV Design. Source: C. Cerimele et al. **A rigid mid lift-to-drag ratio approach to human mars entry, descent, and landing.** AIAA Paper, 2017-1898, 2017.

In their paper, Cerimele et. al [1] provide maximum thrust T_{max} as well as mass, lift and drag characteristics, and other factors important for physical modeling and simulation. The maximum thrust magnitude T_{max} is given as 800 kN , the minimum thrust magnitude T_{min} is 200 kN , and the vehicle's mass at the start of powered descent initiation is $58,000 \text{ kg}$.

The CobraMRV lift and drag coefficients C_L and C_D are modeled based on vehicle Mach number and angle of attack. Vehicle angle of attack is determined directly from the thrust acceleration vector α_T and the vehicle velocity vector \mathbf{V} .

Cerimele et al also provide a reference area S of 62.21 m^2 . Upon ignition, the vehicle's lift and drag are reduced due to the aerodynamic effects of the exhaust plume. This is modeled simply by reducing the reference area to $S/2$. This effect obviously impacts the fuel performance of APDG, but it does not qualitatively affect the performance of Adaptive PDI as will be clear in Chapter 4.

During the unpowered phase of approach when PDI is being optimized, the vehicle is held at a constant angle of attack of 55° to achieve maximum drag.

3.5.2 Atmosphere Model

The atmosphere model is based on NASA's Mars-GRAM 2010 [7], an engineering-level atmospheric model of the Martian atmosphere. The model used for this simulation is an empirically developed equation to represent the Martian atmosphere data within the mission's envelope. Mars-GRAM 2010 is based on NASA Ames Mars General Circulation Model for altitudes under 80 km.

For this simulation, the Mars-GRAM data is used to calculate a density ρ and a speed of sound V_{sound} , from which Mach number is calculated as $\|V\|/V_{sound}$ and lift and drag force magnitudes are calculated as in Equations (3.6) and (3.5), where S is a reference area.

$$L = \frac{1}{2}\rho|V|^2SC_L \quad (3.5)$$

$$D = \frac{1}{2}\rho|V|^2SC_D \quad (3.6)$$

Lift and drag forces are oriented relative to the body axes such that Lift is always in the negative yaw $-\mathbf{body}_Y$ axis shown in Figure 2.1 and defined in Section 3.5.3, and Drag is always in the negative velocity direction $-\hat{\mathbf{V}}$. The \mathbf{F}_{LD} term for numerical integration is therefor given in Equation 3.7

$$\mathbf{F}_{LD} = -L \mathbf{body}_Y + -D \hat{\mathbf{V}} \quad (3.7)$$

A particular feature of the powered descent phase is the change in drag calculation while the engine is ignited. When the guidance system is operating and the rocket is firing, the drag is modeled as half the value computed when the vehicle is unpowered, i.e. during glide. This is due to the rocket plume's aerodynamics. This change is accomplished in the simulation during the PDI phase by simply dividing the reference area by a factor of 2.

3.5.3 Orientation

The vehicle's body Euler angles are computed in a 3-2-1 sequence from the body axes. Since the simulation assumes perfect control, the body axes are computed as

Equations (3.8), (3.9), and (3.10). Pitch, yaw, and roll are then calculated as the angles between the body axes and the planet-fixed guidance frame \hat{e} . Angle of attack is similarly calculated using the body axes and the velocity vector. The CobraMRV's configuration determines that the thrust acceleration vector be in the direction of the vehicle yaw axis.

$$\mathbf{body}_Y = \mathbf{a}_T / \|\mathbf{a}_T\| \quad (3.8)$$

$$\mathbf{body}_P = \frac{\mathbf{r} \times \mathbf{body}_Y}{\|\mathbf{r} \times \mathbf{body}_Y\|} \quad (3.9)$$

$$\mathbf{body}_R = \mathbf{body}_Y \times \mathbf{body}_P \quad (3.10)$$

3.6 MONTE CARLO

The Monte-Carlo script calls the PD Sim with simulation settings, vehicle parameters, initial condition, and navigation uncertainty. This allows each individual run to have dispersed conditions without modification of the code. The Monte-Carlo script allows choice of initial condition, fixed or Adaptive PDI, as well as specification of rocket parameter dispersion, initial condition dispersion in position and velocity, and navigation noise distribution.

The Monte-Carlo script is designed to allow testing of various scenarios and includes initial condition selection among a set of cases. The cases simulated here are points along a trajectory that passes nearly over the landing site, simulating the trajectory resulting from a typical re-entry and aerobraking glide phase. These cases also include initial velocity information that coincides with the vehicle having traveled unpowered along its trajectory. In fixed initial condition mode the user specifies which initial conditions to test, the initial states are dispersed, and the simulations are run from the dispersed starting conditions. In Adaptive PDI mode, the Monte-Carlo script automatically chooses the nominal starting condition as the first point along this trajectory. It then performs the number of runs specified by the user and disperses the starting point each run according to dispersion specifications.

The dispersion factors are chosen to reflect realistic parameter dispersion. Navigation error is modeled using a normal (Gaussian) distribution with standard

deviations in accordance with Moesser's 2010 [13] work as described in Section 3.4. Rocket parameter dispersion is modeled as a uniform distribution of 2% of the parameter. Initial condition values are normally distributed about their nominal values. The dispersion is applied such that three standard deviations in position dispersion is 1000 m from the mean, and three standard deviations in velocity dispersion is 10 m/s from the mean. The simulated navigation error is modeled as normally distributed noise as well with 3 m at the 3σ level for position and 1 m/s for velocity in each axis. These distributions are all tabulated in Table 3.1, with the Gaussian distributions described using the 3σ convention representing the range which encompasses $\approx 99.7\%$ of resulting values.

Parameter	Distribution	3σ	Width
IC Position	Gaussian	1000 (m)	
IC Velocity (kg)	Gaussian	10 (m/s)	
Nav Position Noise	Gaussian	3 (m)	
Nav Velocity Noise	Gaussian	1 (m/s)	
m_0	Uniform		2%
T_{max} & T_{min}	Uniform		2%
v_{ex}	Uniform		2%

Table 3.1. Monte-Carlo Dispersion Settings

Each rocket parameter dispersion is modeled as uniform, and each state dispersion is modeled as Gaussian. Only the nominal rocket parameters and dispersed navigation values can be known to the guidance computer, and the modular design allows this distinction to be made easily. The simulation script calls the guidance computer with nominal max thrust and the guidance computer outputs a throttle setting based on that nominal value, but the simulation script applies thrust limits based on the real dispersed values.

The separation between nominal and dispersed rocket parameters is also important to the PDI strategy, ideally performed within the guidance computer. The PDI required acceleration criterion is implemented as in Algorithm (2), but the guidance

computer only has the nominal maximum thrust available to it. Similarly, it only has the dispersed navigation values available for the range criterion in Algorithm (3).

The Monte-Carlo script maintains repeatable randomness for testing. Each of the individual runs starts with a seed to the simulation environment’s random number generation algorithm such that re-running the simulation with the same seed will produce precisely identical results. This pseudo-random quality allows investigation of particular runs and helps the software development cycle immensely. The run seeds are stored directly with the run result data in a table so that if later evaluation shows an oddity that should be examined, the run can quickly be replicated.

3.7 INITIAL CONDITION

The initial conditions are listed in Table 3.2. These are representative of a trajectory of the CobraMRV vehicle on approach after a de-orbit burn and subsequent targeting, from the work of Cerimele et al [1]. They are provided in the guidance frame \hat{e} , which is oriented such that the origin is at the final landing site, \hat{e}_x is pointed “East”, \hat{e}_y is pointed “North”, and \hat{e}_z is pointed “Up”. The simulation itself runs in a Mars-centered Mars-fixed frame.

Table 3.2. Initial Conditions for Mars Landing.

State	Case	\hat{e}_x	\hat{e}_y	\hat{e}_z	Unit
r_0	6	6079	-30720	8685	m
V_0	6	-121.0	644.1	-64.82	m/s
r_0	5	5013	25170	8054	m
V_0	5	-121.1	616.5	-78.57	m/s
r_0	4	3947	-19860	7305	m
V_0	4	-120.9	589.6	-91.67	m/s
r_0	3	2887	-14790	6444	m
V_0	3	-120.1	563.3	-103.9	m/s
r_0	2	2359	-12,340	5973	m
V_0	2	-119.7	550.2	-109.7	m/s
r_0	1	1832	-9949	5478	m
V_0	1	-119.8	537.0	-115.4	m/s

These conditions represent an entry trajectory that is slightly off-target for the landing site and requires both powered deceleration to avoid overshoot as well as redirection to correct the angle error. The trajectory traveled from the furthest starting condition (Case 6) unpowered in a vacuum is plotted in Figure 3.3 along with the starting positions for Cases 1 through 6 indicated by an X. Similarly, Figure 3.5 shows the trajectory in atmosphere with the vehicle held at the optimum angle of attack (55°). Figure 3.4 shows the trajectory error in terms of ground range to landing site as the vacuum trajectory passes over the site at around 48 seconds.

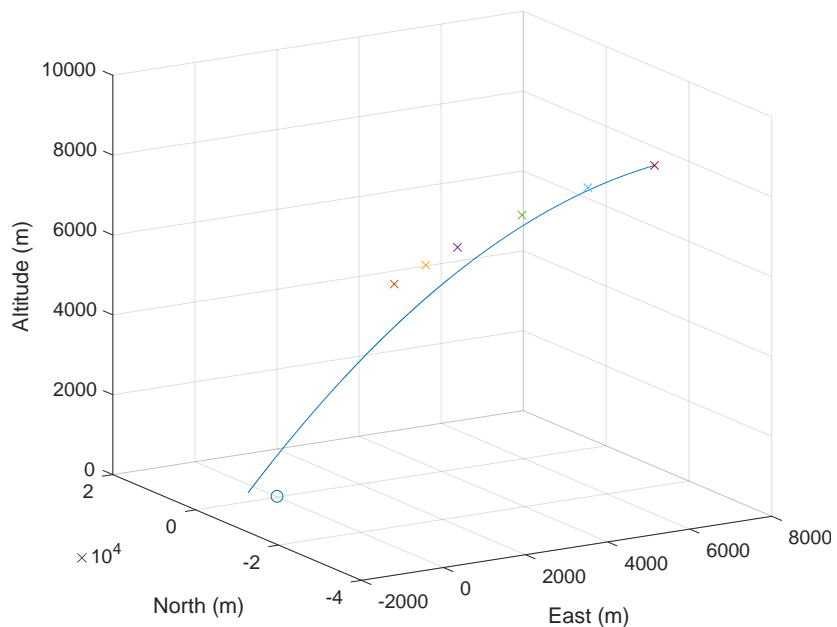


Figure 3.3. Unpowered Initial Trajectory in Vacuum

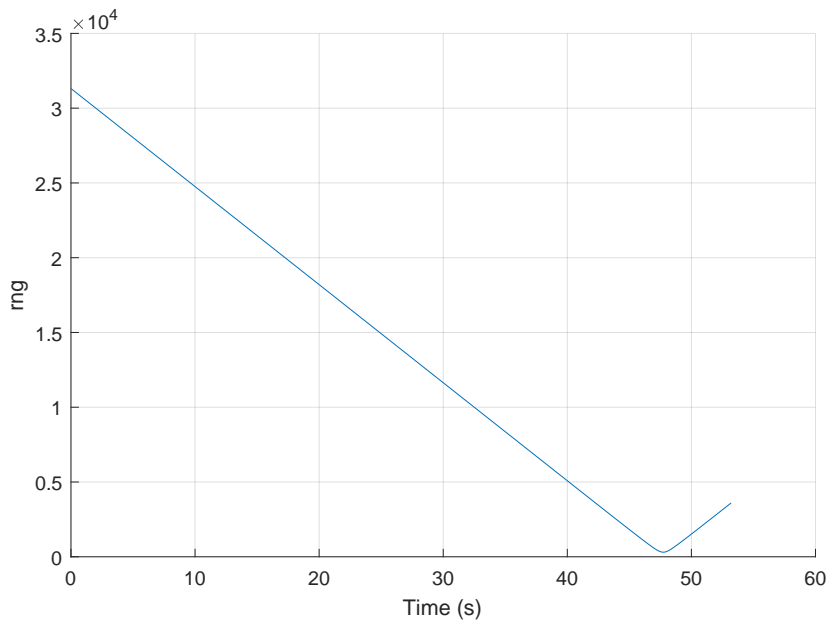


Figure 3.4. Ground Range: Unpowered Initial Trajectory In Vacuum

As is clear from Figures 3.5 and 3.6 by the placement of the initial conditions of the 6 cases, the initial conditions are chosen to represent the landing vehicle on aerodynamic approach making corrections toward the site. While employing the PDI strategy outlined in Section 2.4 the vehicle will travel along the atmospheric trajectory shown in Figures 3.5 and 3.6 until ignition.

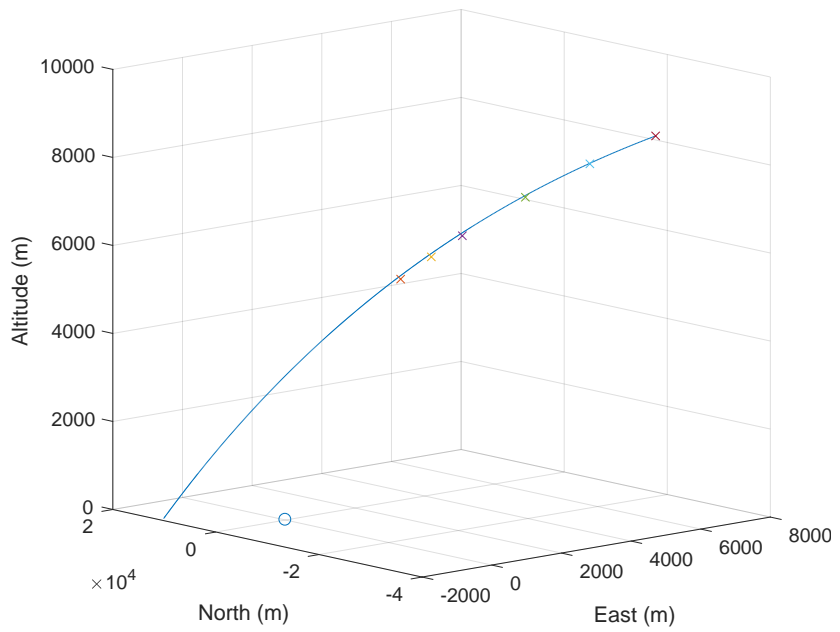


Figure 3.5. Unpowered Initial Trajectory in Atmosphere

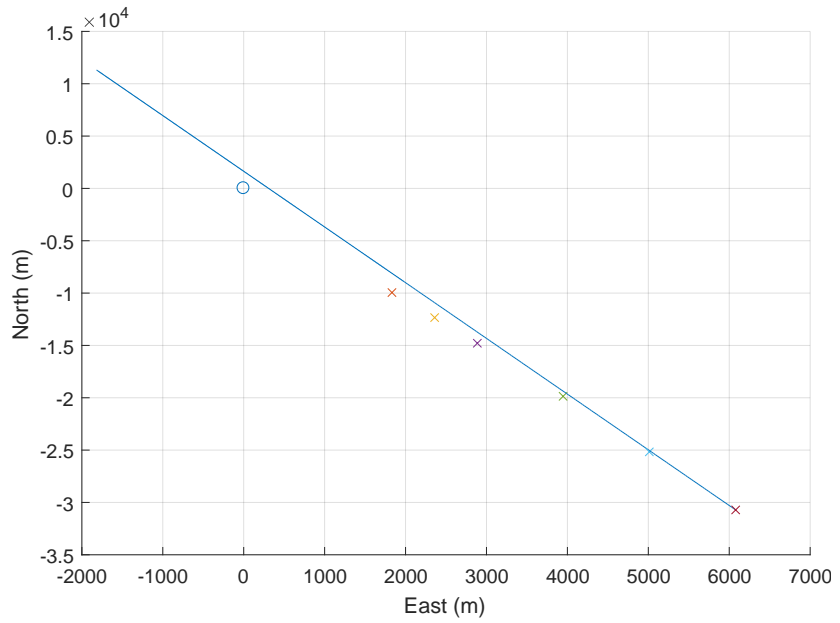


Figure 3.6. Unpowered Initial Trajectory in Atmosphere From Above

CHAPTER 4

RESULTS

In this chapter, results are presented for several simulated conditions.

1. Nominal vs. dispersed parameters
2. Atmosphere vs. vacuum
3. Static initial conditions vs. Adaptive PDI

The first condition, the effect of dispersion, is of interest on the topic of robustness. A closed-loop guidance law implementation is intended to ensure satisfaction of the problem constraints in practical conditions with uncertainty of state and performance limitations. A guidance system without periodic state feedback, i.e. an open-loop implementation, would be expected to quickly lose accuracy and ultimately fail in real application. Due to the criticality of safety in the intended mission, it is vital to show that the Adaptive PDI strategy performs well in nominal as well as dispersed conditions and to give a sense for the uncertainty in its performance.

The second condition is of particular interest because, as is clear in Section 2.3, neither APDG nor the PDI strategy take into account atmospheric effects and, at least in the case of the Apollo missions, have not been flown in the context of atmospheric landing. It is important to verify that the strategy can satisfy mission goals and still perform well in atmosphere, and the comparison with vacuum conditions serves both as a control as well as a fuel requirement baseline.

The third condition is the subject of this study. Whether Adaptive PDI can reliably provide propellant efficiency improvement while maintaining safety and practicality is the topic of interest.

For dispersed cases the starting conditions are as listed in Table 3.2 with the addition of Case 7, which represents the active PDI strategy. This Case is flown from the

initial condition specified by Case 6, the first point on the trajectory, but with the engine off until one of the PDI criteria defined in Equations (2) and (3) is met.

4.0.1 Adaptive PDI

The first result to investigate is the validity of the PDI criteria in Equations (2) and (3). For these criteria to serve as ignition criteria, they must reliably trigger in time to land the vehicle softly.

Figure 4.1 shows data from a vacuum case of APDG with PDI active during the unpowered phase, before PDI has been triggered. The required thrust acceleration magnitude a_{GT} for a gravity turn is shown monotonically increasing throughout the unpowered trajectory, and the required downrange travel s_{GT} is monotonically decreasing. a_{GT} and s_{GT} reach their limits at almost the same time, but this would not be true of all trajectories.

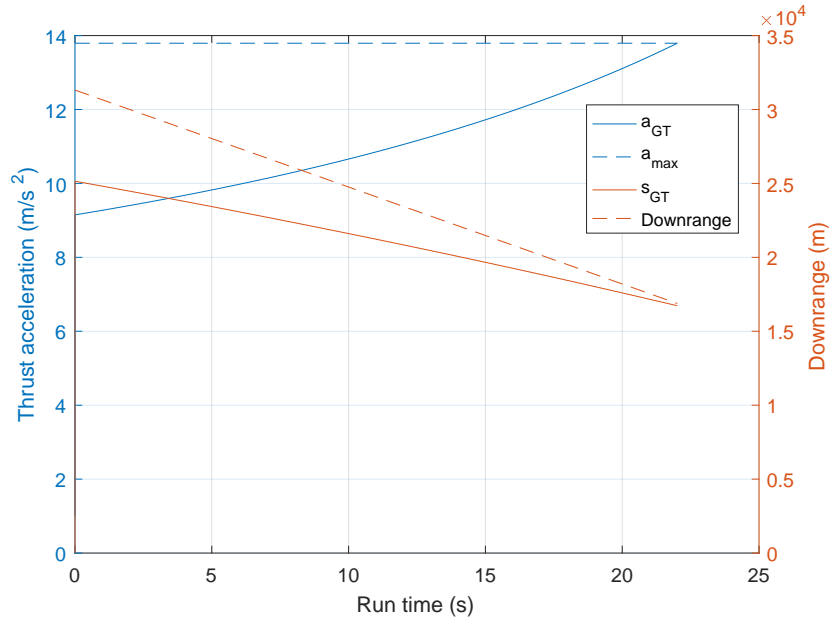


Figure 4.1. PDI Criteria: Vacuum

Figure 4.2 shows data from an atmospheric case of APDG with PDI active during the unpowered phase, before PDI has been triggered. Here the required thrust

acceleration a_{GT} is still monotonically increasing but not as quickly as it did in a vacuum, while s_{GT} is decreasing similarly quickly. This behavior is examined in Section 4.0.4, where it is clear in Figures 4.16 and 4.18 that the vehicle is able to provide significant lift while decelerating through drag during the unpowered phase in atmosphere. Figure 4.2 clearly shows that the risk of overshoot, reflected in the downrange criterion, is much greater than exceeding the maximum thrust acceleration for this trajectory in atmosphere.

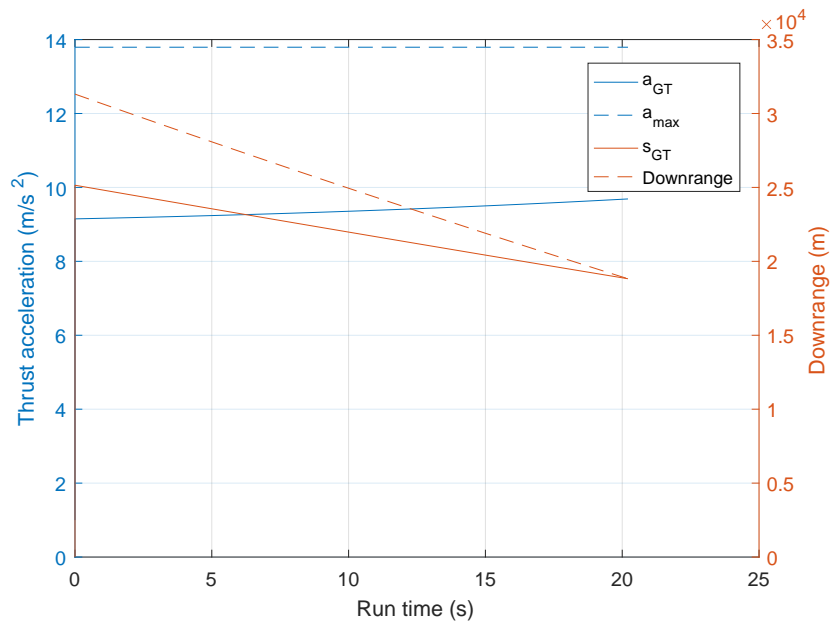


Figure 4.2. PDI Criteria: Atmosphere

4.0.2 Comparison of E-Guidance with APDG

The choice between E-Guidance of Equation (2.29) as flown on the Apollo missions and APDG of Equation (2.32) is examined below. Results are first presented as nominal performance in atmosphere in order to investigate the individual performance of each law without the effects of dispersion. Beyond this section, results will be presented using APDG.

Figures 4.3 through 4.8 show plotted quantities of a rocket in atmosphere employing the PDI strategy on approach to landing at the origin from Initial Condition

Case 6 (Table 3.2). In Figure 4.3 the trajectory with the steeper approach upon landing is flown by APDG.

The laws each result in similar trajectories as evidenced by Figures 4.3 through 4.6. However, the thrust profiles are notably different, with the APDG trajectory starting at a lower magnitude of thrust in Figure 4.7 than E-Guidance and their profiles roughly reversed. The pitch angle profiles in Figure 4.8 are very different with APDG providing a final pitch angle much closer to zero, indicating a level touchdown.

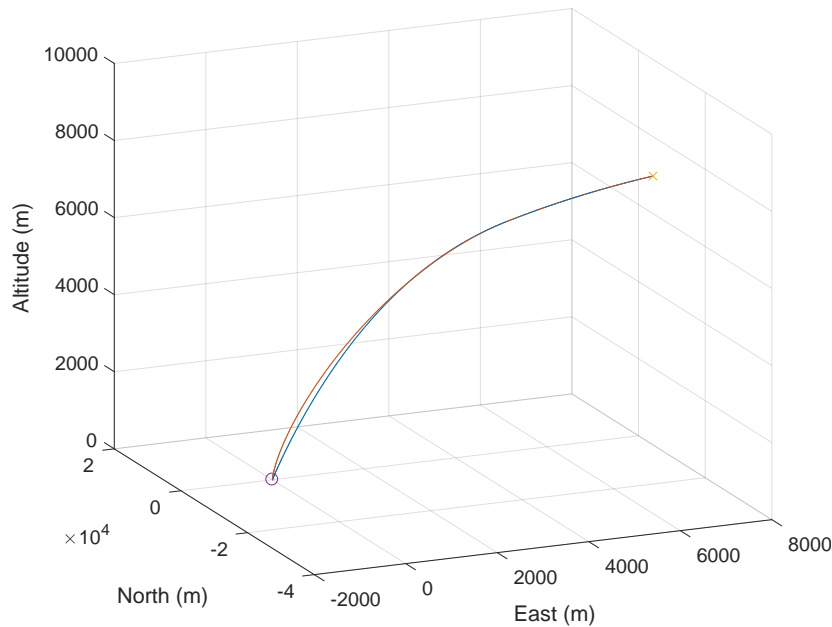


Figure 4.3. Trajectory: E-Guidance vs. APDG

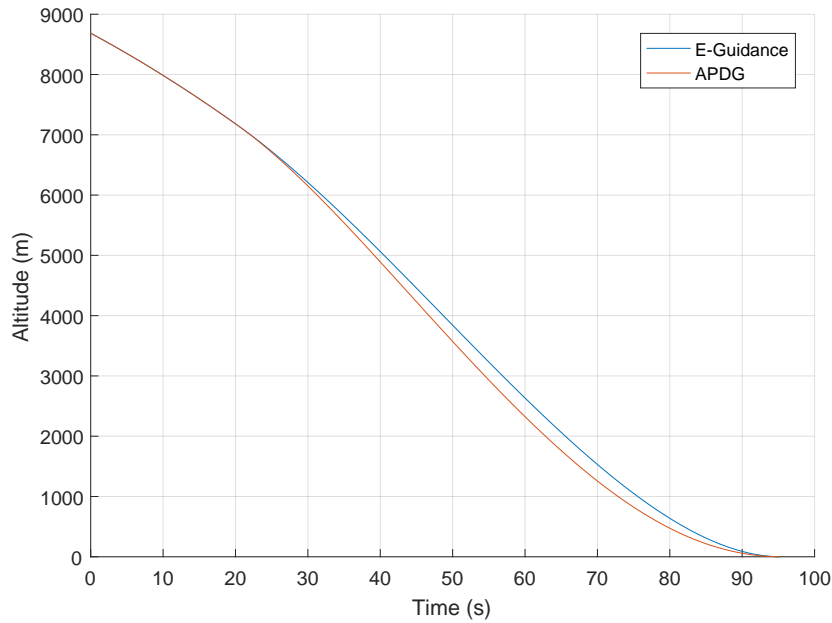


Figure 4.4. Altitude: E-Guidance vs. APDG

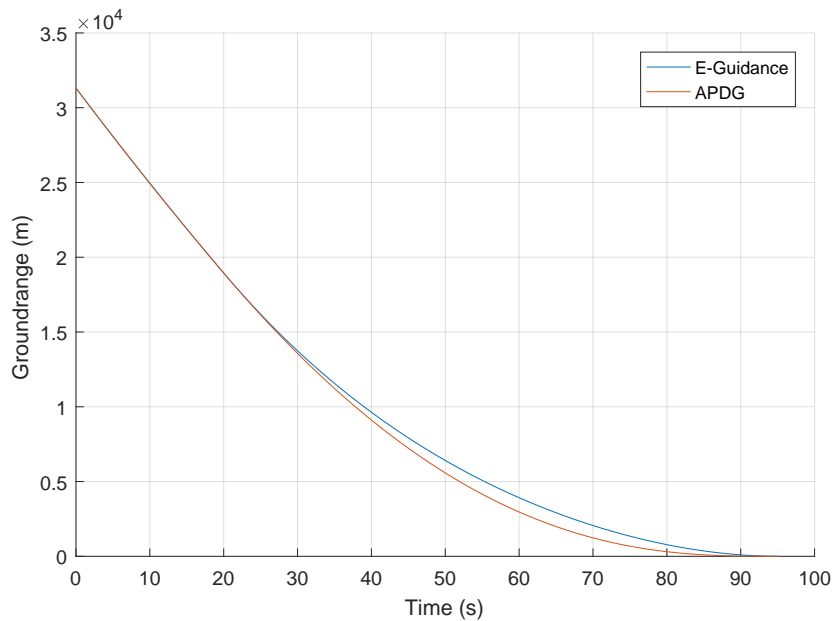


Figure 4.5. Ground Range: E-Guidance vs. APDG

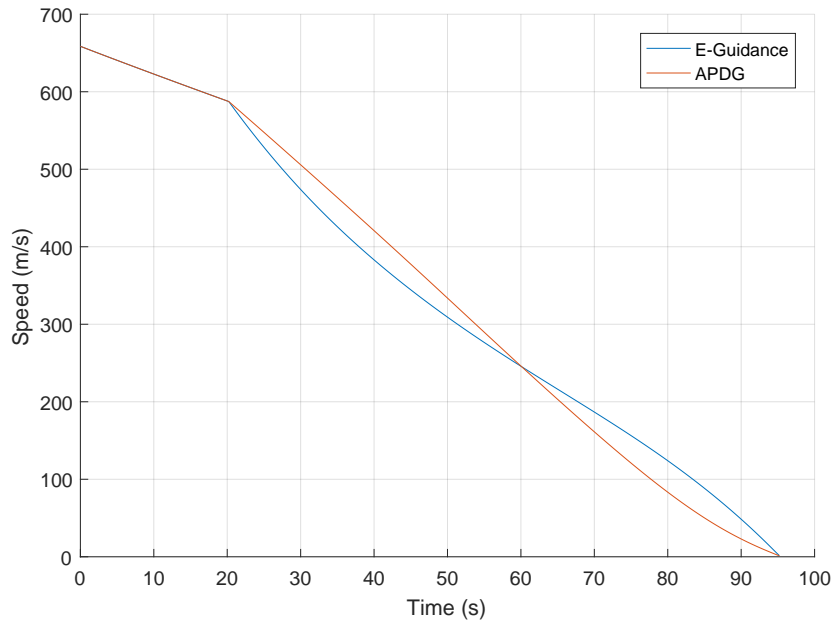


Figure 4.6. Speed: E-Guidance vs. APDG

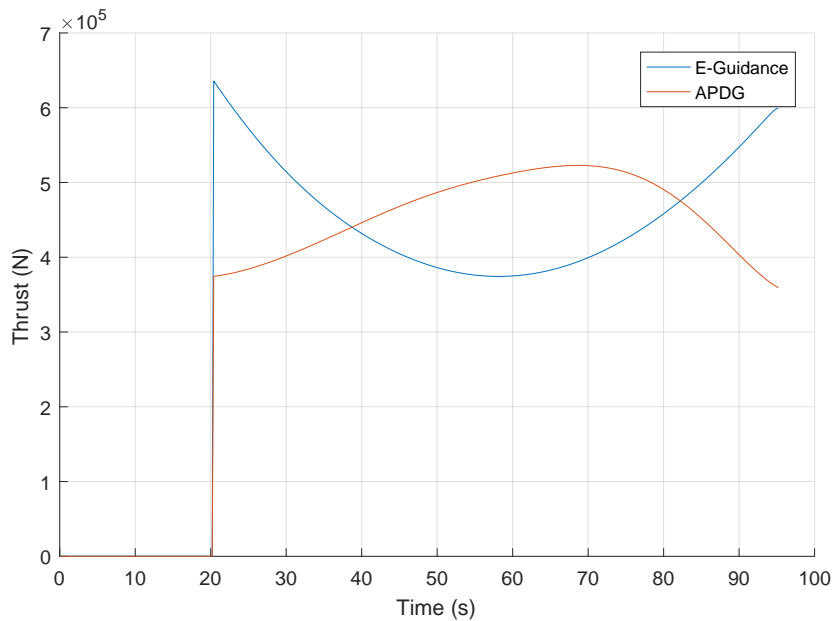


Figure 4.7. Thrust Magnitude: E-Guidance vs. APDG

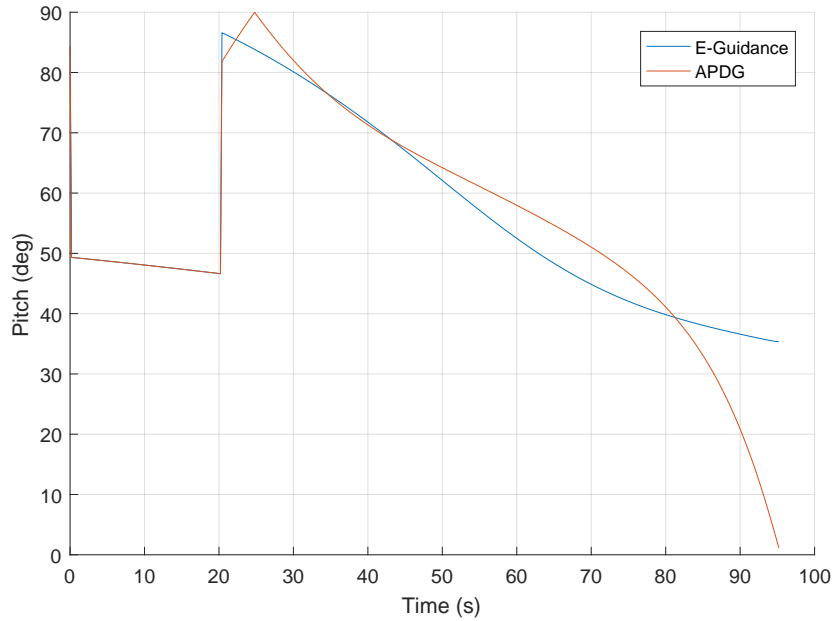


Figure 4.8. Pitch: E-Guidance vs. APDG

Including dispersion results in similar profiles which will be examined more closely in later sections, but a numerical comparison of the laws' performance is given in Table 4.1. Each law was in control for 1000 runs. Results are presented as mean values and standard deviations σ . Both laws perform similarly with the APDG law showing slightly higher speed on landing and using more fuel. This speed inaccuracy will be addressed in Section 4.0.3.

Guidance Law	E-Guidance	APDG
Runs	1000	1000
Fuel (kg)	9707.4	9849.8
Fuel σ	280.1	287.3
Fuel max	10665.2	10698.2
Fuel min	8792.3	8924.6
Flight Time (s)	95.2	95.0
FT σ	2.0	2.0
FT max	102.3	101.5
FT min	88.9	88.4
Range (m)	1.9	2.5
Range σ	1.5	1.9
Range max	8.4	8.8
Range min	0.0	0.0
Speed (m/s)	5.9	8.0
Speed σ	3.1	3.6
Speed max	14.9	15.5
Speed min	0.4	0.3

Table 4.1. Comparison of Performance of E-Guidance with APDG

These parameters give bounds on the results, but do not provide much information on the underlying distributions. What we see in histograms of the data in Figure 4.9 is that fuel consumption for both E-Guidance and APDG follows a normal distribution fairly well, with APDG using slightly more fuel on average. Figures 4.10 and 4.11 do not show normal distributions, with Range heavily weighted toward zero and Speed being much less centrally organized.

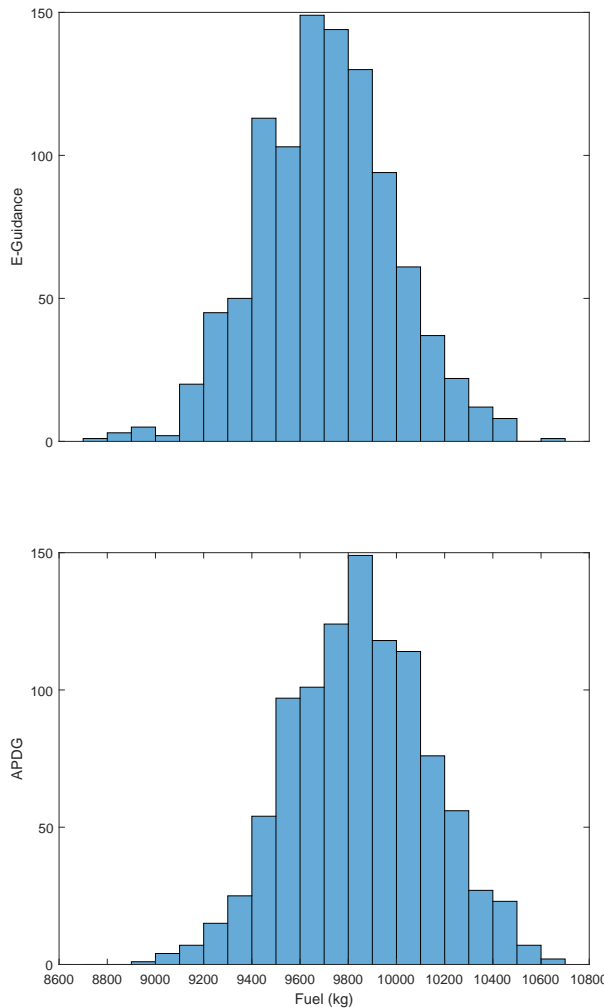


Figure 4.9. Propellant Use Distribution: E-Guidance vs. APDG

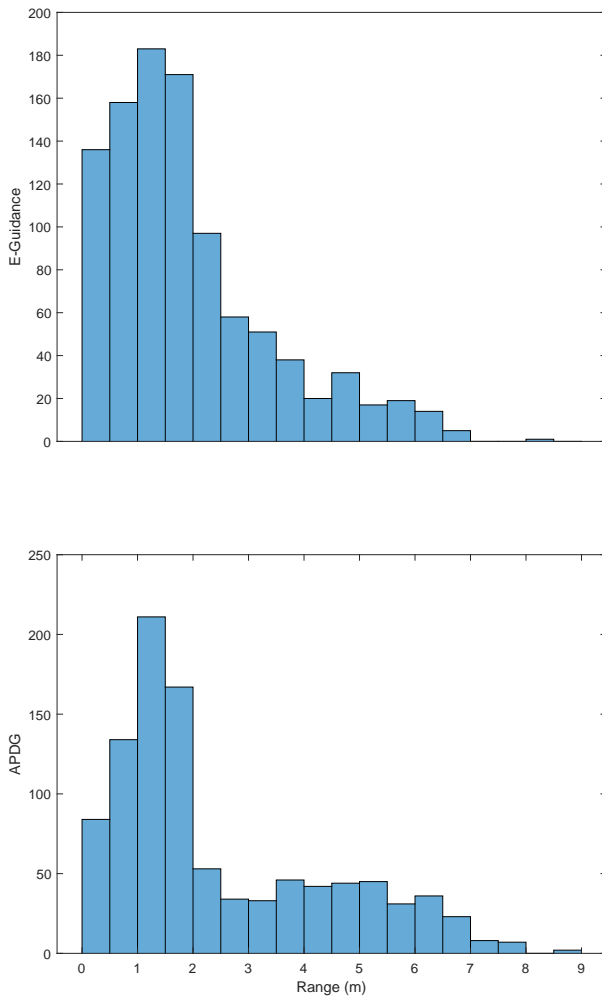


Figure 4.10. Ground Range Distribution: E-Guidance vs. APDG

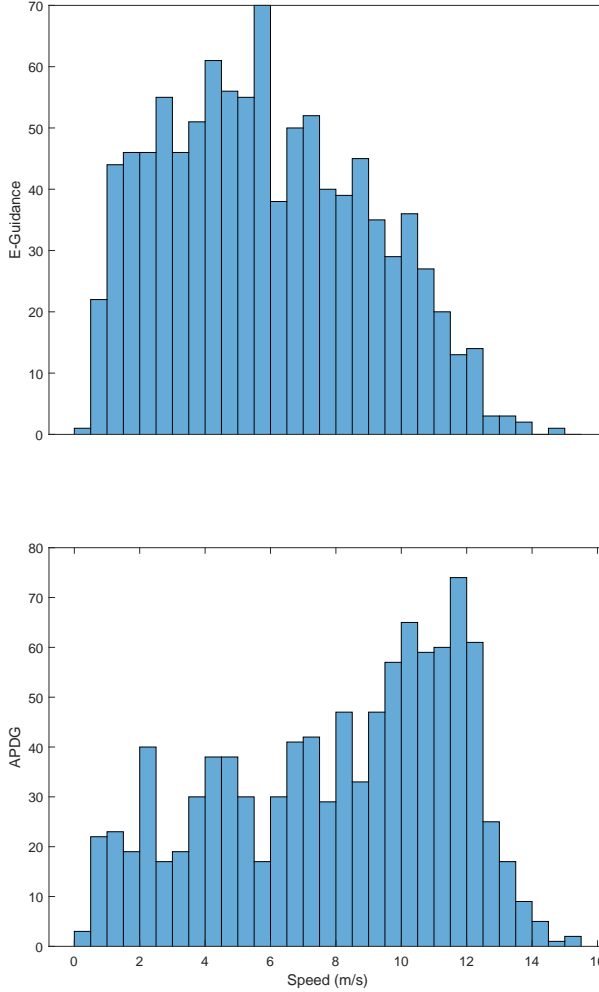


Figure 4.11. Speed Distribution: E-Guidance vs. APDG

4.0.3 Navigation Error

The final speeds shown in Table 4.1 are not very accurate given the terminal velocity constraint magnitude of 1 m/s . This constraint is important since it determines how softly the vehicle will land. However, this final speed (and range) inaccuracy is due almost entirely to the navigation dispersion model outlined in Section 3.4, as is clear from the results given in Table 4.2. Here the simulation was run with atmospheric effects, PDI,

and full initial condition and rocket parameter dispersion. The cases differed only in whether navigation dispersion was active. The Nominal runs show very accurate satisfaction of the terminal constraints in spite of the guidance update stop for the last half second. A higher fidelity model would include much lower navigation error near the landing site due to the availability of more accurate measurements through radar systems and short-range devices and would result in similarly low inaccuracies. More sophisticated sensor models are not investigated here since they would only apply near the end of flight, resulting in little impact on fuel consumption or performance of the PDI strategy.

Navigation	Nominal	Dispersed
Runs	1000	1000
Fuel (kg)	9761.8	9849.8
Fuel σ	270.8	287.3
Fuel max	10526.1	10698.2
Fuel min	8939.5	8924.6
Flight Time (s)	95.2	95.0
FT σ	2.0	2.0
FT max	102.5	101.5
FT min	89.0	88.4
Range (m)	0.1	2.5
Range σ	0.0	1.9
Range max	0.2	8.8
Range min	0.0	0.0
Speed (m/s)	1.0	8.0
Speed σ	0.0	3.6
Speed max	1.1	15.5
Speed min	1.0	0.3

Table 4.2. Performance of APDG With and Without Navigation Error

Histograms of the data show more clearly the effects of Navigation error. Figure 4.12 still shows a normal distribution of propellant use for both Dispersed and

Nominal cases. Figure 4.10 however gives a sharp contrast between the two conditions. The Dispersed case is identical to the APDG plot in Figure 4.10 (as it shows the same data) with a lopsided distribution of final Ground Range. The Nominal case is a single vertical bucket, indicating that all 1000 runs were within 0.5 m of the landing site. Table 4.2 indicates that they were all within 0.2 m. The landing speed shown in Figure 4.14 tells a similar story with slightly higher error in the nominal case than in Ground Range.

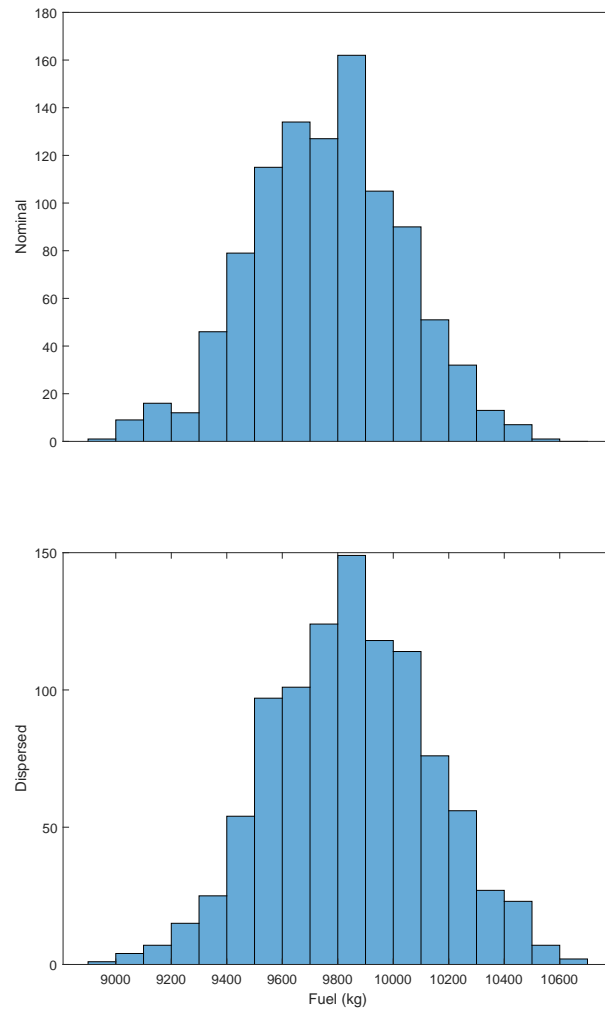


Figure 4.12. Propellant Use Distribution: Nominal vs. Dispersed Navigation

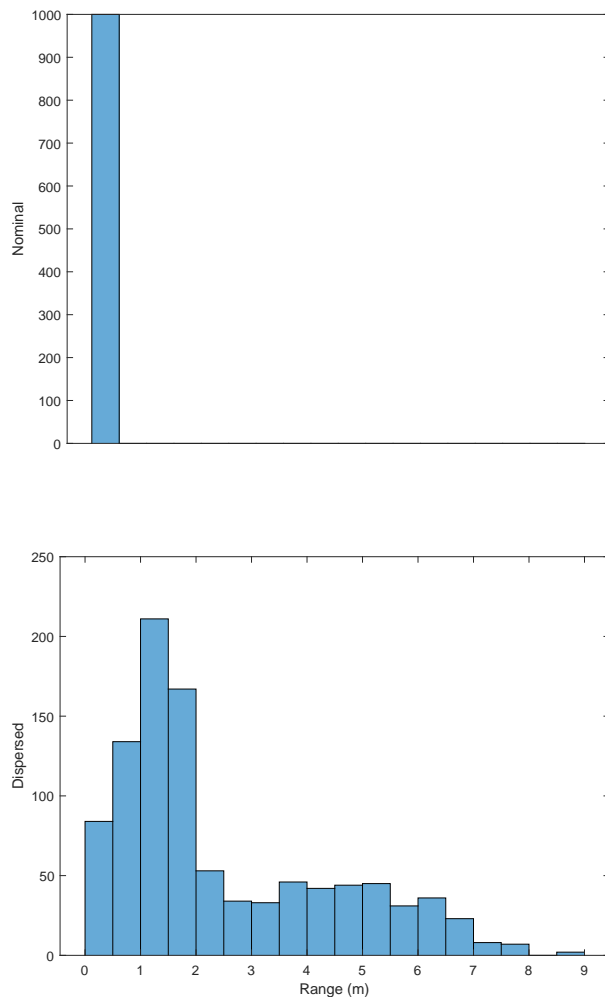


Figure 4.13. Ground Range Distribution: Nominal vs. Dispersed Navigation

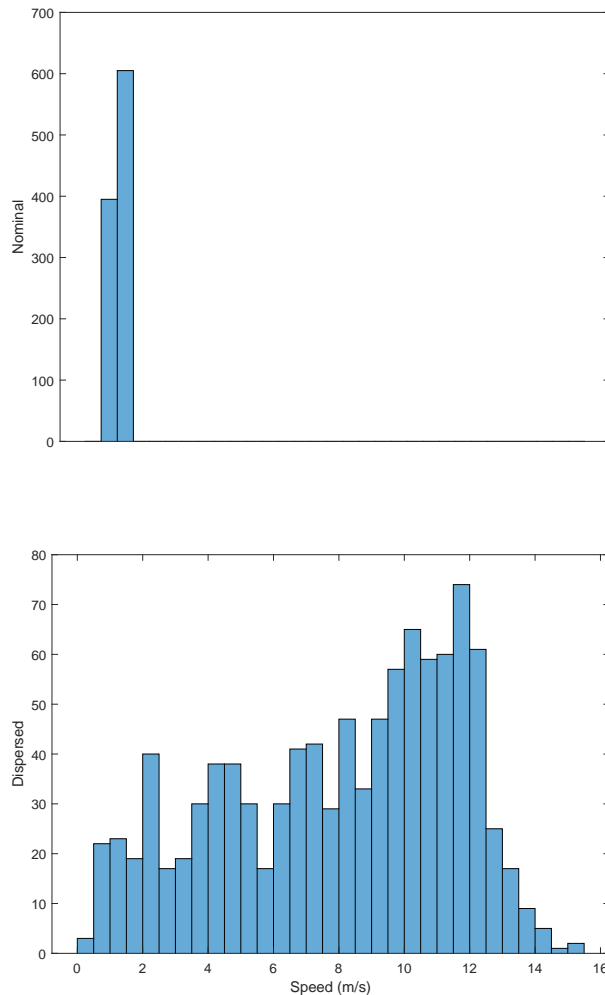


Figure 4.14. Speed Distribution: Nominal vs. Dispersed Navigation

4.0.4 Vacuum vs. Atmosphere

Here APDG's performance is compared with and without aerodynamic effects. This is an important comparison to make because, as stated in Section 2.3.1, the guidance law is derived without consideration of aerodynamic effects. There is no guarantee it will perform well in atmosphere. Only nominal results will be presented here, as the dispersed

results are presented in Sections 4.0.5 and 4.0.6 in the context of adaptive powered descent initiation (PDI) vs. predetermined ignition time.

Figures 4.15 through 4.20 show nominal profiles for the APDG law in both atmosphere and vacuum. These trajectories start from Case 6 as listed in Table 3.2. Figures 4.15 and 4.16 show that in atmosphere, the PDI strategy with the vehicle held at optimum angle of attack results in higher lift, meaning that the vehicle does not lose altitude as quickly as in vacuum, while Figure 4.18 shows it losing speed much more quickly during this phase. This suggests that the aerodynamic effects have an appreciable effect on the energy in the form of propellant ultimately required for powered descent and soft landing.

Figures 4.19 and 4.20 suggest the same conclusion. Upon ignition, the thrust required in atmosphere is far lower than that required in vacuum, and the Vehicle Mass stays higher in atmosphere throughout most of the trajectory, particularly the ending mass, reflecting lower fuel consumption. The thrust profile in atmosphere suggests a fairly conservative ignition; since more energy is burned off through aerodynamic effects, less thrust is required than might be expected by the gravity turn solution which generates the operative time-to-go. This leaves an appreciable margin for error which is explored further in the dispersed results of Section 4.0.6.

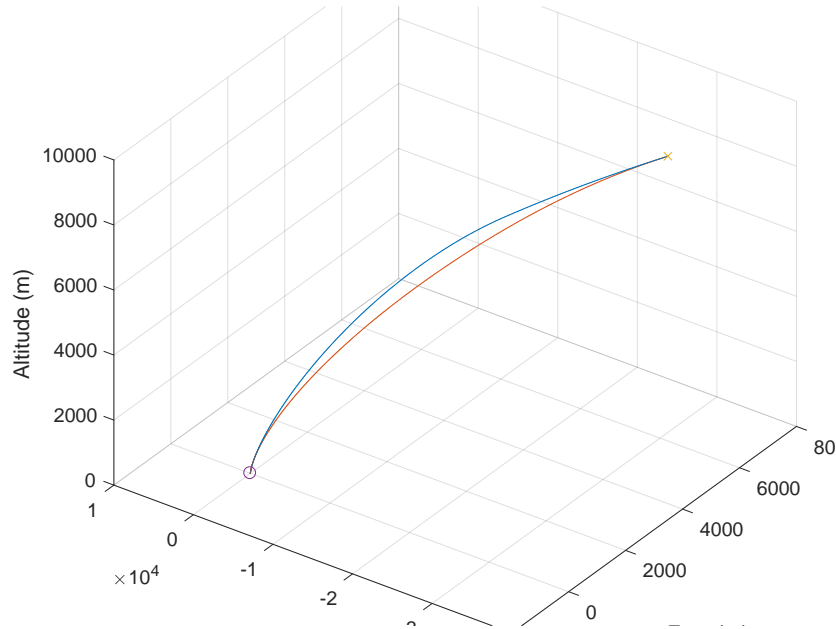


Figure 4.15. Trajectory: Vacuum vs. Atmosphere

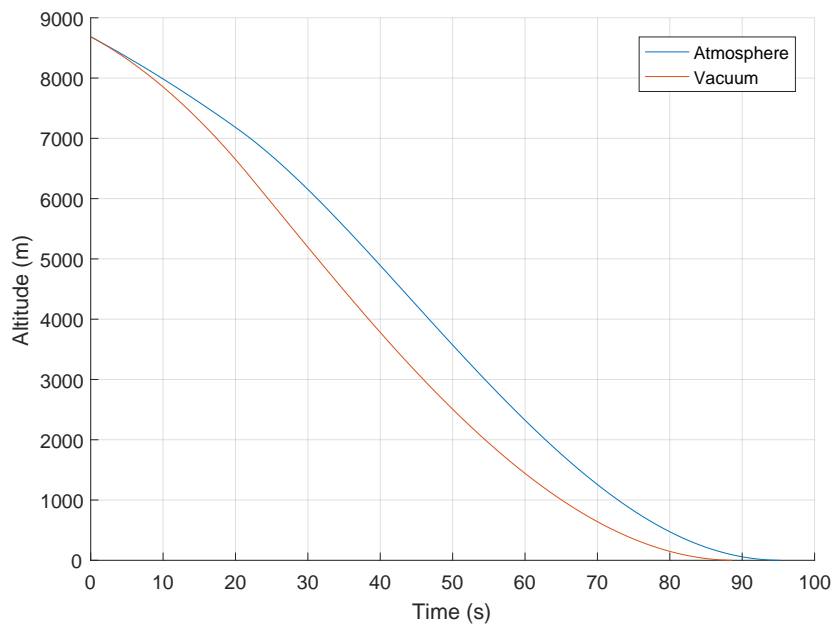


Figure 4.16. Altitude: Vacuum vs. Atmosphere

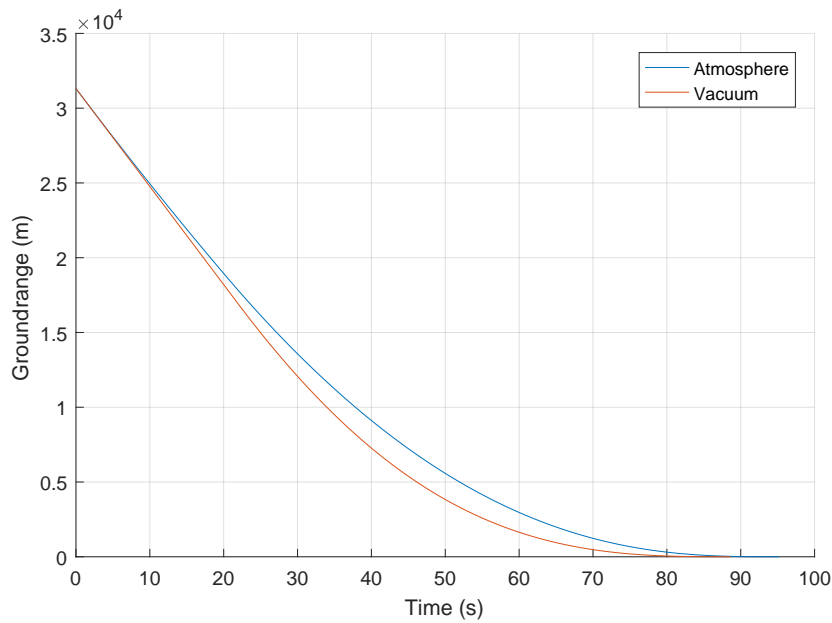


Figure 4.17. Ground Range: Vacuum vs. Atmosphere

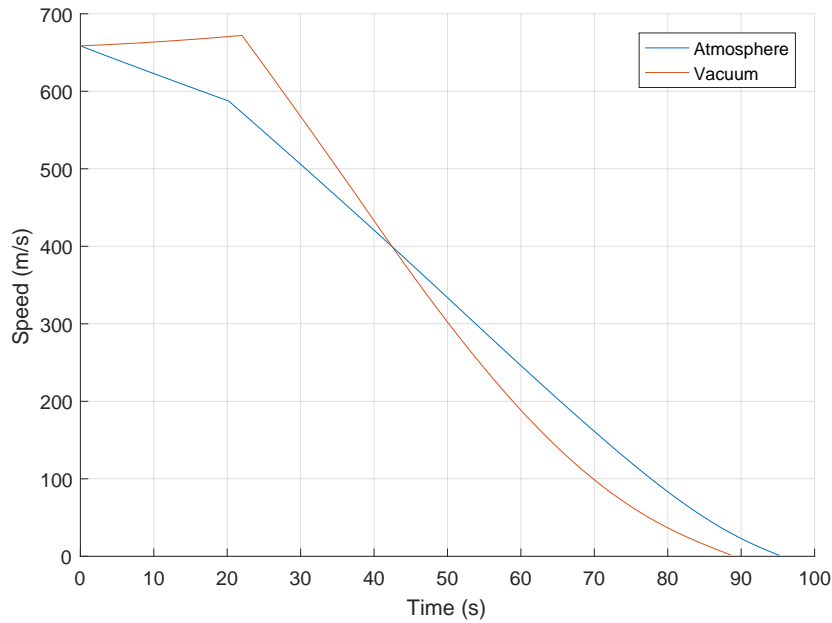


Figure 4.18. Speed: Vacuum vs. Atmosphere

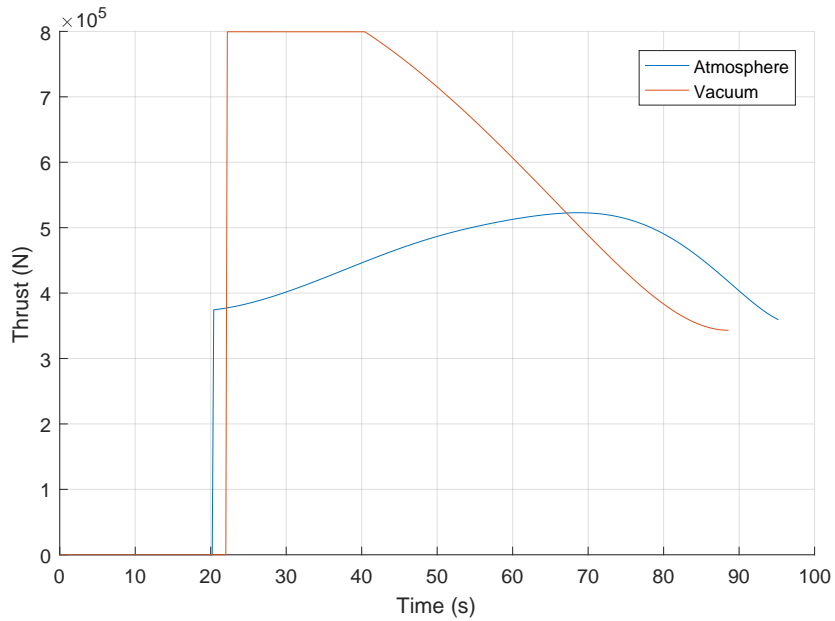


Figure 4.19. Thrust Magnitude: Vacuum vs. Atmosphere

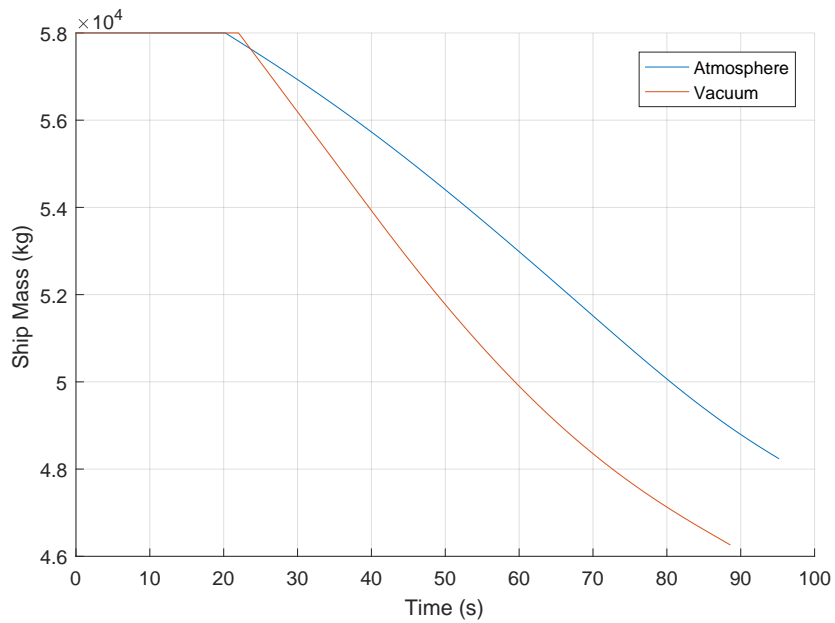


Figure 4.20. Vehicle Mass: Vacuum vs. Atmosphere

4.0.5 Vacuum Performance

Presented here are results for the vacuum condition, comparing the performance and robustness of APDG with Adaptive PDI against specified ignition time in the form of predetermined initial conditions for a mission without aerodynamic effects. This is similar to the conditions experienced by the Apollo missions, though the simulation's parameters reflect a Martian gravitational field. As discussed in Section 3.2, there is a 1.2 safety factor applied to the time-to-go as provided by Equation (2.33) upon ignition for all cases in vacuum.

Figures 4.21 through 4.25 show nominal results for all cases. This gives a baseline from which to evaluate the typical profiles of each Case and the PDI strategy.

Figure 4.21 shows significant landing site overshoot on Case 1. The plot of Ground Range vs. Time in Figure 4.24 tells a similar story, with the ground range nearly reaching zero before increasing at around 30 seconds before settling back toward zero. Figure 4.25 is the most telling plot, with the Thrust Magnitude profiles for each case plotted vs. time. Cases 4 through 6 do not saturate at any point in their trajectories, either at the lower or upper bounds of thrust. Cases 1 through 3 do, however, with Case 1 saturating at the upper bound for a large portion of its trajectory.

Case 7 representing the PDI strategy also saturates its thrust for part of its trajectory after ignition but settles out toward the middle of the range by the end of its flight. Its other plots are unique relative to the other cases as well, with Speed in Figure 4.22 showing the characteristic increase in speed due to its ballistic trajectory until powered descent initiation, unlike all other Cases. Its Altitude in Figure 4.23 starts in line with Case 6 but decreases more quickly and ends on a similar path as Case 4. Its Ground Range behaves similarly in Figure 4.24. Its trajectory in Figure 4.21 stands out in red, clearly following a much different path than any of the other Cases.

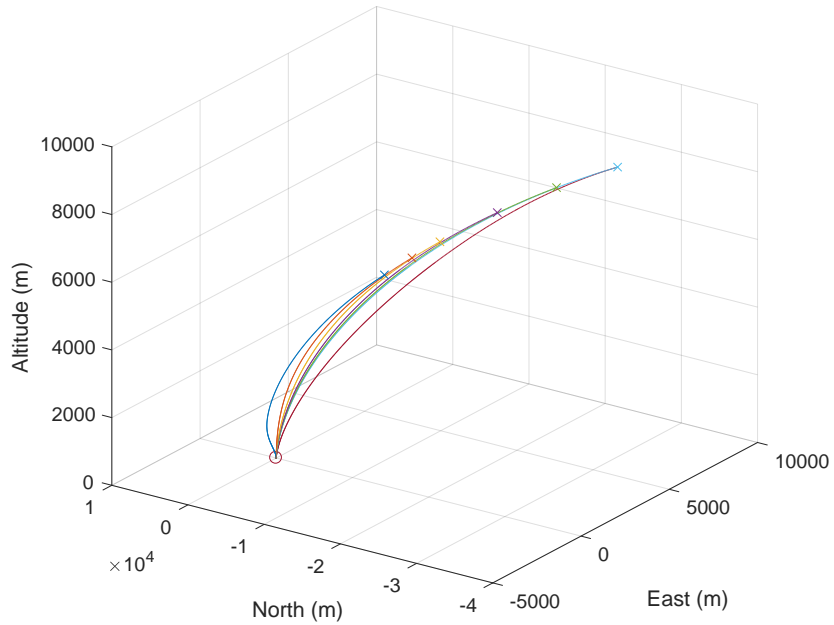


Figure 4.21. Trajectory: APDG in Vacuum

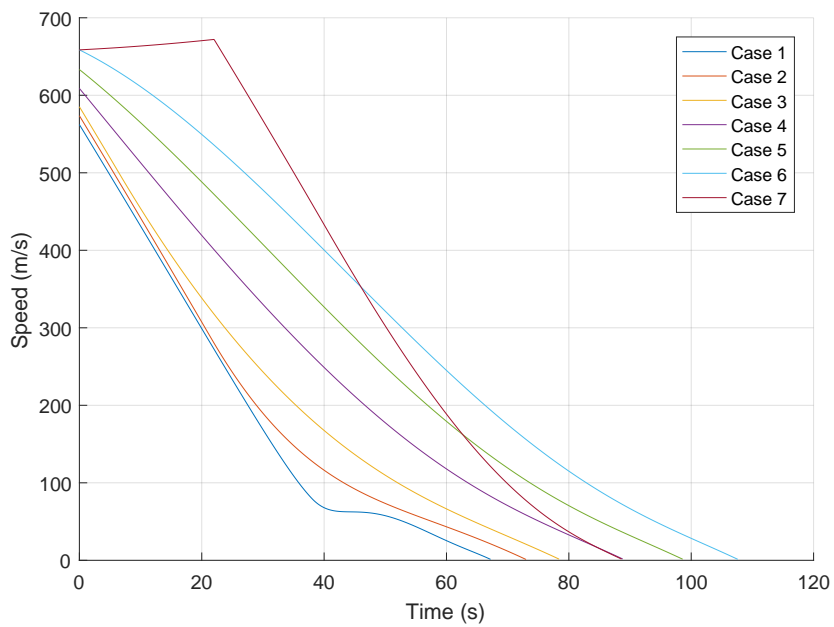


Figure 4.22. Speed: APDG in Vacuum

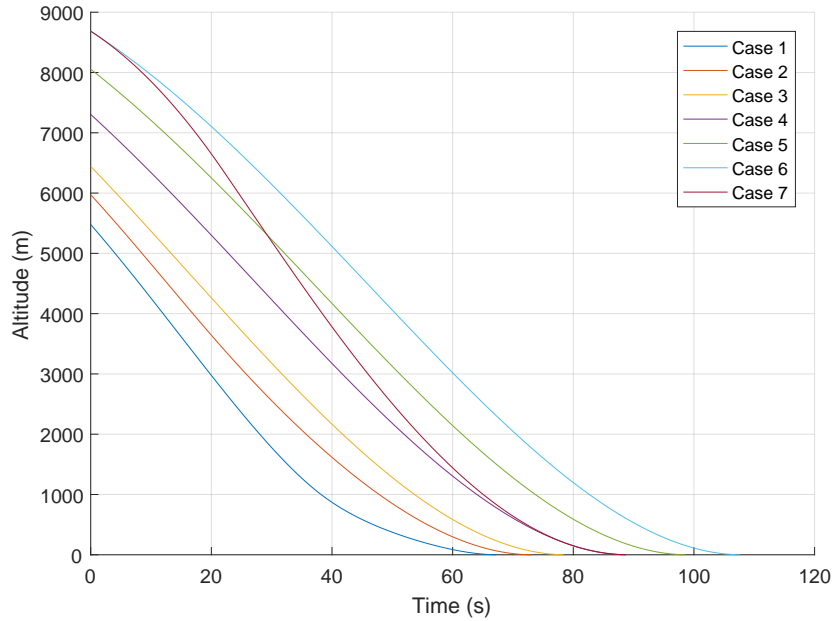


Figure 4.23. Altitude: APDG in Vacuum

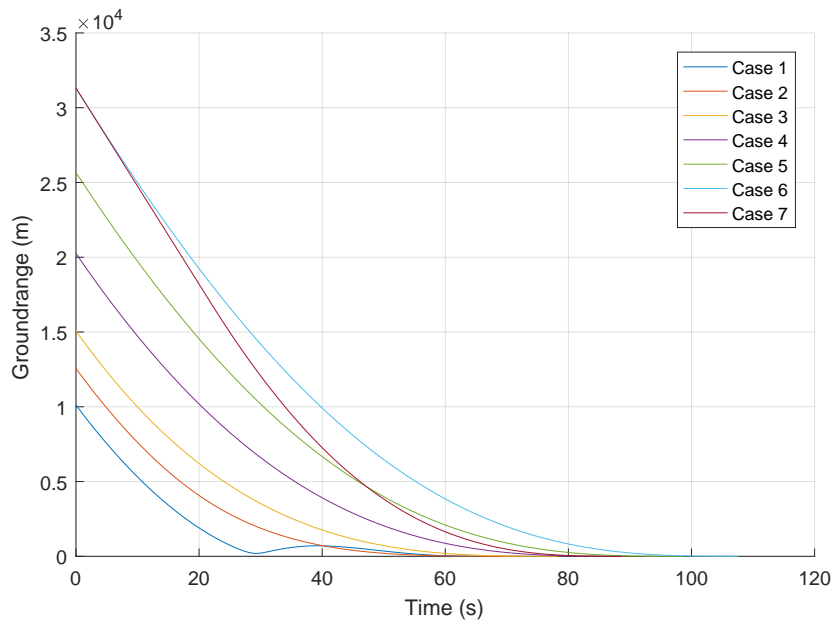


Figure 4.24. Ground Range: APDG in Vacuum

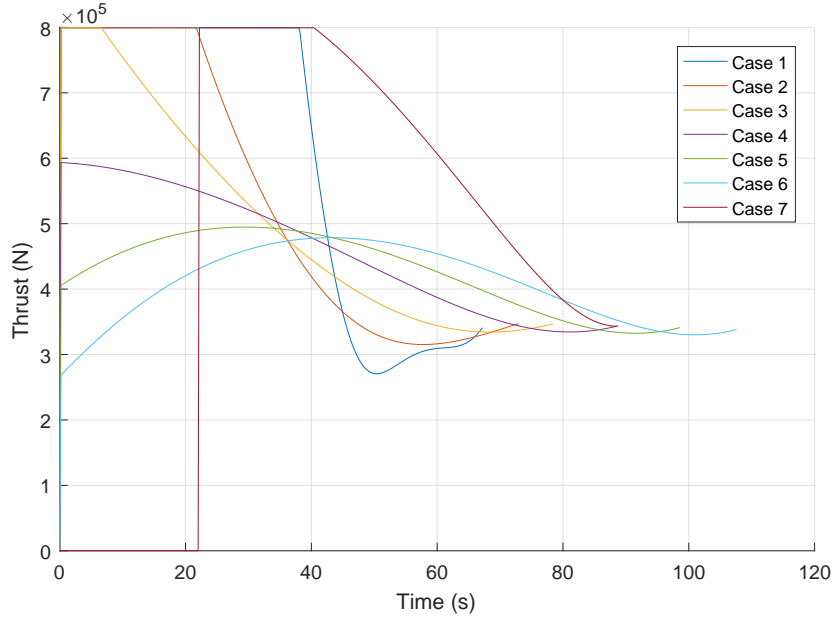


Figure 4.25. Thrust Magnitude: APDG in Vacuum

Introducing dispersion gives the results in Table 4.3. Most of the Cases perform similarly in terms of deviation from the mean aside from Case 1. Case 1 shows much higher fuel consumption deviation, flight time deviation, final range deviation, and final speed deviation.

These deviations are due to failed landings; fully 45 of the 1000 runs of Case 1 in vacuum failed to land softly. All other runs had final ranges below 16 m, and all 45 of these failed landings had final ranges of over 500 m as shown in Figure 4.26, the landing site location distribution. Similarly, the 45 failed landings had final speeds in excess of 90 m/s, compared to the 16 m/s for all other Case 1 runs shown in Figure 4.28. Since the standard deviations of the other successful cases are in line with the errors expected from Navigation uncertainty in Section 4.0.3, 16 m/s can be considered a bound on the error due to Navigation uncertainty, so these 45 landings are clearly cases where the guidance system failed.

None of the other cases had any such landing failures.

The lowest mean propellant consumption is given by Case 2, as well as the highest standard deviation in propellant consumption aside from Case 1.

Case	1	2	3	4	5	6	7
Runs	1000	1000	1000	1000	1000	1000	1000
Fuel (kg)	11650.1	11184.7	11264.0	11634.4	12032.7	12436.7	11885.2
Fuel σ	605.8	308.2	264.9	247.0	259.6	241.9	257.9
Fuel max	13482.2	12306.1	12188.7	12330.1	12936.5	13189.6	12706.8
Fuel min	8258.6	10078.8	10495.6	10977.1	11230.6	11710.8	11123.6
Flight Time (s)	66.0	72.7	78.3	88.9	98.6	107.7	90.1
FT σ	5.7	3.4	3.1	3.1	3.1	3.0	3.7
FT max	79.1	83.3	89.1	99.1	108.5	116.9	109.5
FT min	37.6	63.2	69.0	78.2	88.7	97.2	82.4
Range (m)	54.3	2.5	2.5	2.6	2.7	2.5	2.7
Range σ	244.5	2.0	2.0	2.0	2.1	2.1	2.0
Range max	1789.8	8.4	8.7	9.3	9.6	8.8	10.4
Range min	0.0	0.0	0.0	0.0	0.0	0.0	0.0
Speed (m/s)	11.5	8.3	8.0	8.3	8.5	8.3	8.4
Speed σ	15.8	3.7	3.7	3.8	3.7	3.8	3.7
Speed max	110.1	15.4	15.4	15.7	16.1	15.8	17.0
Speed min	0.7	0.3	0.5	0.3	0.5	0.5	0.7

Table 4.3. Performance of APDG In Vacuum

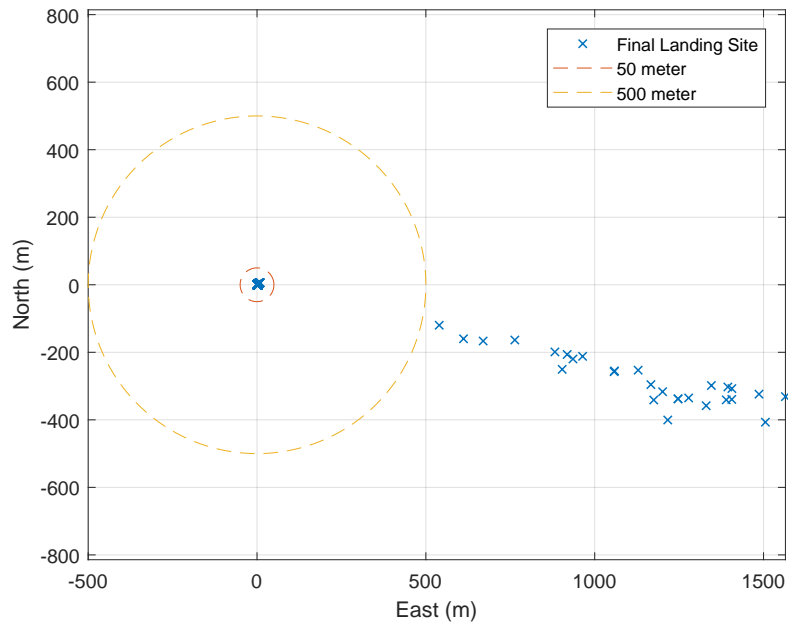


Figure 4.26. Case 1 Landing Sites: APDG in Vacuum

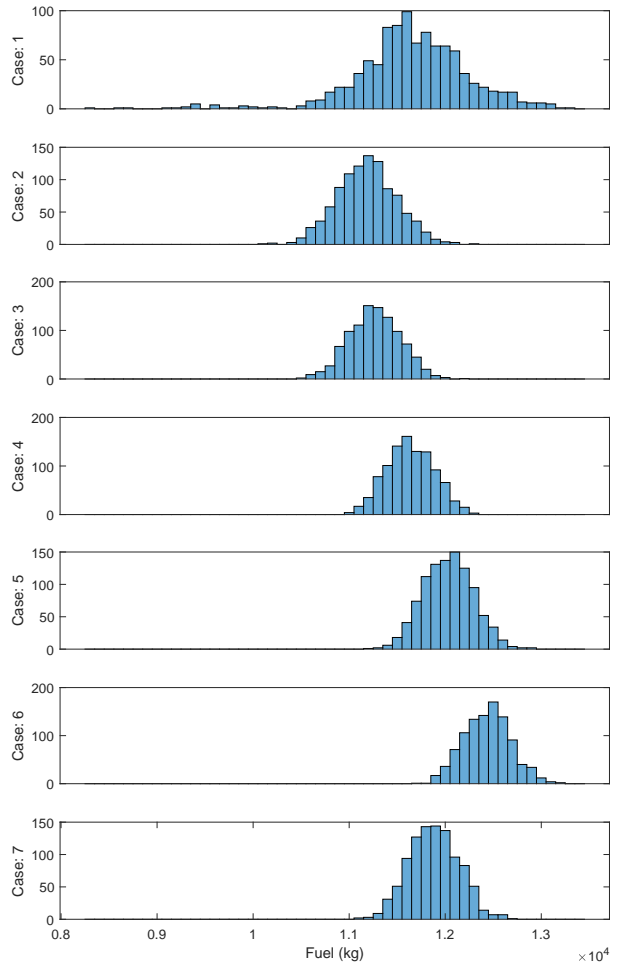


Figure 4.27. Fuel Histogram: APDG in Vacuum

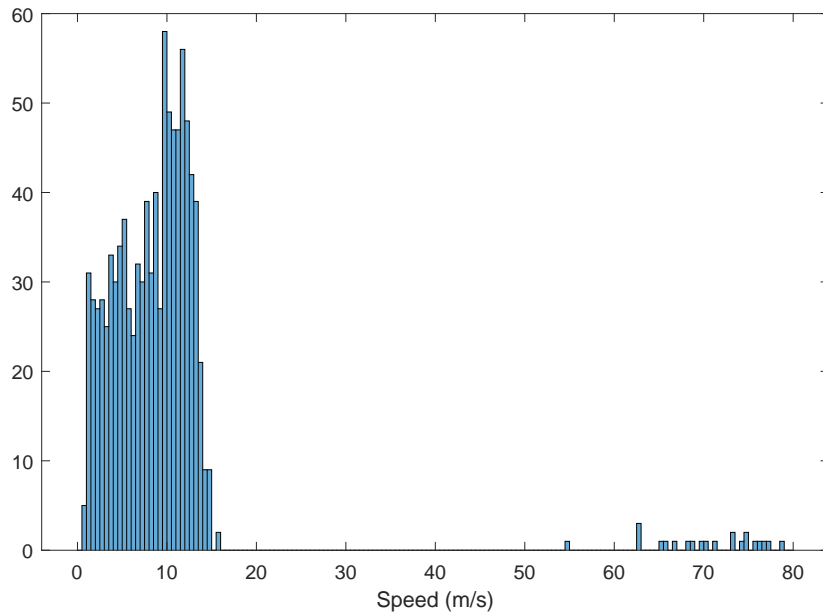


Figure 4.28. Failures Histogram: APDG in Vacuum

The histogram data similarly shows Adaptive PDI's fuel performance as middling in Figure 4.27. It also demonstrates the Gaussian characteristic of the propellant usage distribution. Speed and Range histograms are shown in the Appendix as they are very similar to the relationship demonstrated in Section 4.0.3, with the exception of Case 1. As discussed, Figure 4.27 shows the failures of Case 1 very clearly with the disorderly grouping below 16 m/s representing successful landings, but the much higher speeds shown with a wide separation from the successes. These failures also correspond to the uncharacteristically low propellant runs in Figure 4.27.

4.0.6 Atmospheric Performance

Presented here are results for the atmospheric condition, comparing the performance and robustness of APDG with Adaptive PDI against specified ignition time in the form of predetermined initial conditions for a mission with aerodynamic effects. This is representative of a Martian mission, the intended purpose of the CobraMRV. As

discussed in Section 3.2, there is no safety factor applied to the time-to-go as provided by Equation (2.33) upon ignition for any case in atmosphere.

Figures 4.29 through 4.33 show nominal trajectories from each of the 6 Cases outlined in Table 3.2 as well as Case 7 representing the Adaptive PDI strategy from the starting condition of Case 6. Figures 4.30 and 4.32 show the behavior discussed in Section 4.0.4 in which PDI's unpowered glide retains altitude while shedding speed. Figure 4.32 also shows odd behavior in Case 6, explained easily by Figure 4.33 in which the thrust saturates on the lower bound. Figure 4.33 shows PDI operating in the middle of the thrust range throughout the trajectory after ignition.

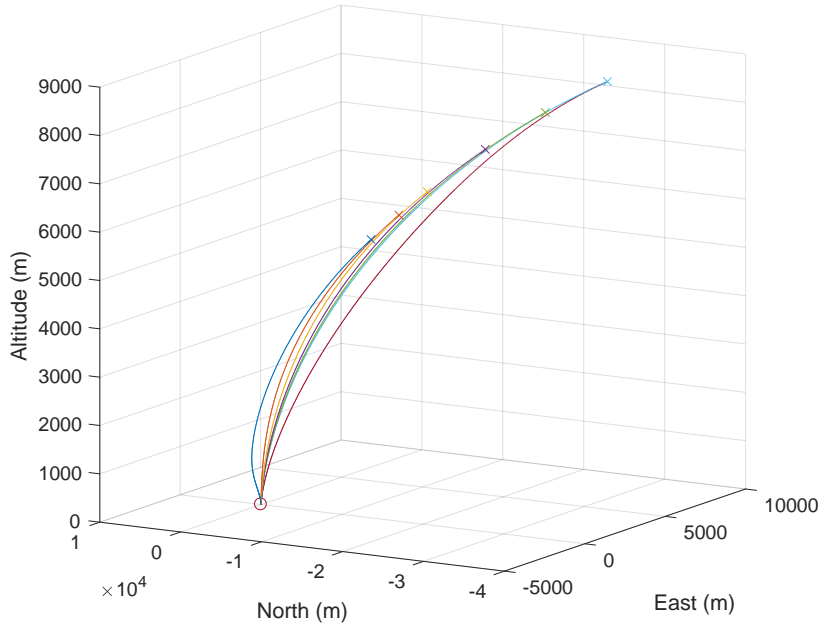


Figure 4.29. Trajectory: APDG in Atmosphere

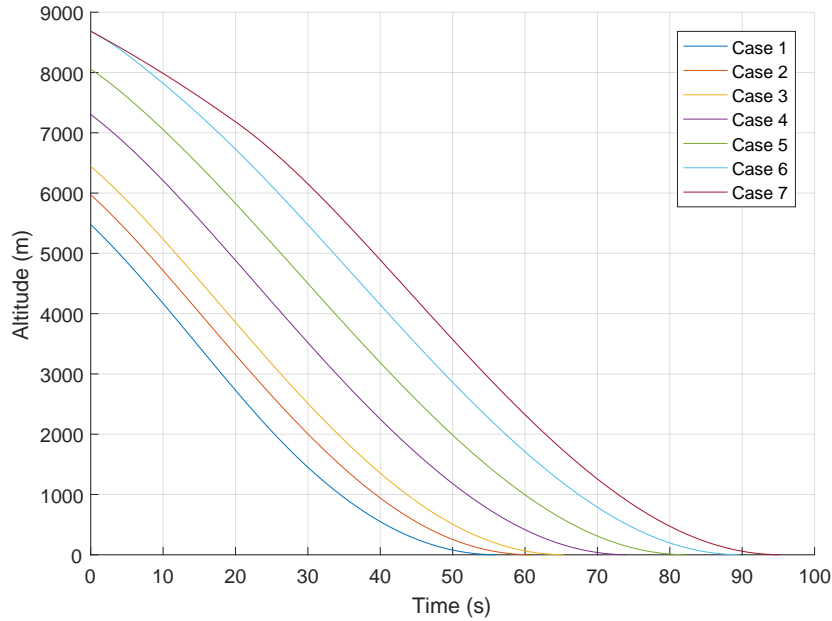


Figure 4.30. Altitude: APDG in Atmosphere

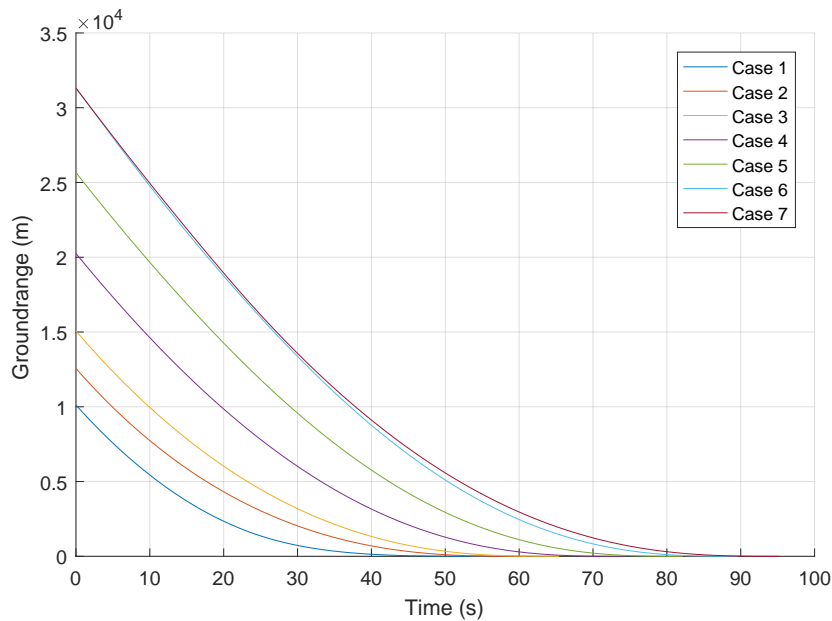


Figure 4.31. Ground Range: APDG in Atmosphere

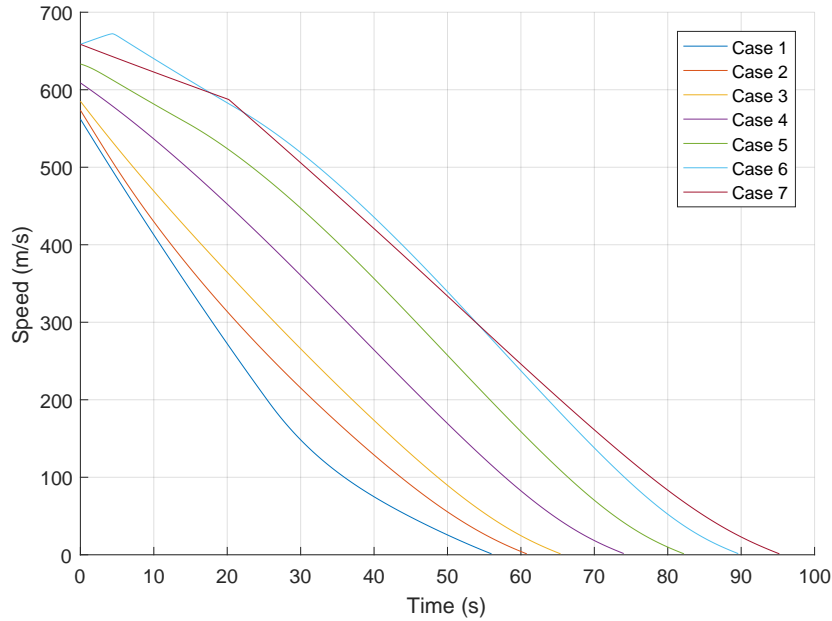


Figure 4.32. Speed: APDG in Atmosphere

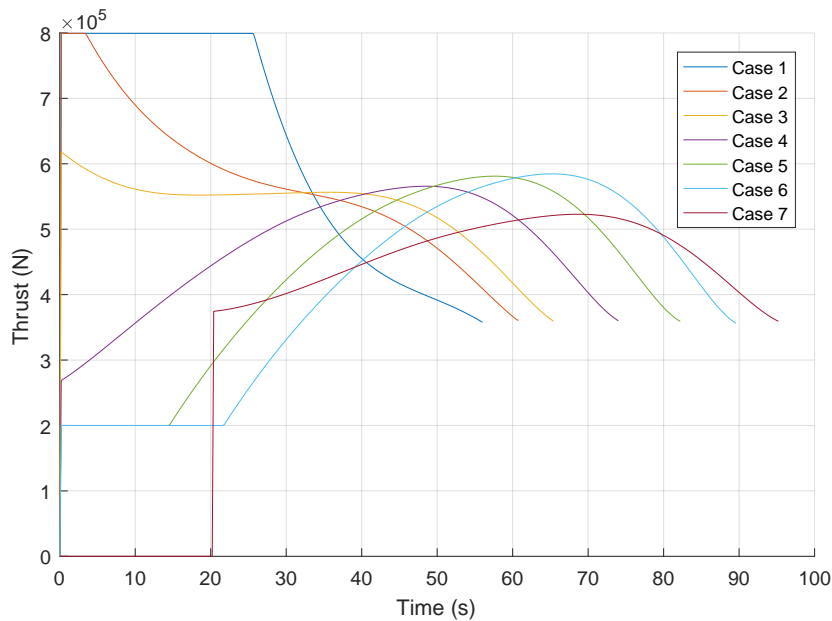


Figure 4.33. Thrust Magnitude: APDG in Atmosphere

Introducing dispersion produces Table 4.4. Again we see Case 1 showing failed landings. In atmosphere only 13 landings of 1000 failed, with range misses in excess of 200 m as shown in Figure 4.34 and speeds in excess of 32 m/s. These values are lower than in vacuum, though still represent an unacceptable level of risk for a manned mission.

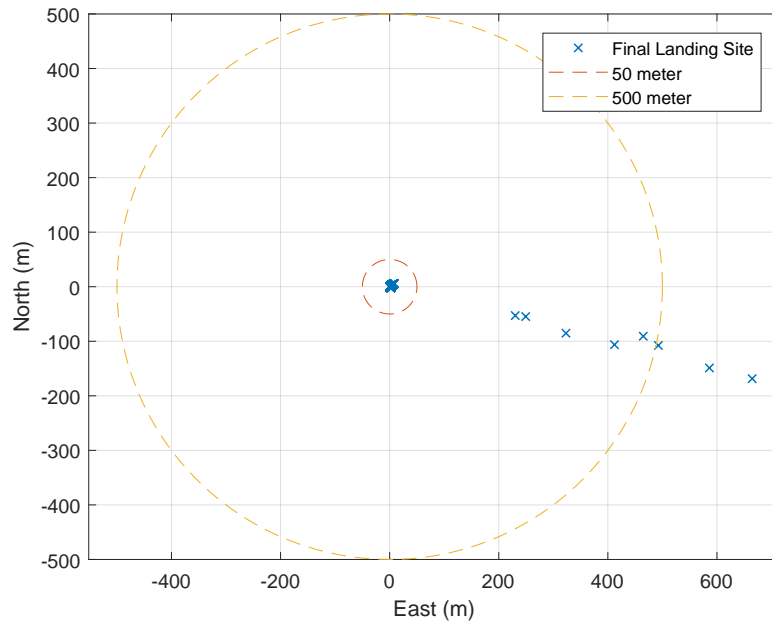


Figure 4.34. Case 1 Landing Sites: APDG in Atmosphere

PDI shows the best propellant performance in atmosphere and no landing failures. Its final range and speed accuracy is well in line with the other Cases and the error introduced by Navigation uncertainty discussed in Section 4.0.3.

Case	1	2	3	4	5	6	7
Runs	1000	1000	1000	1000	1000	1000	1000
Fuel (kg)	10141.2	9947.4	9918.5	9900.6	10010.2	10413.7	9849.8
Fuel σ	357.5	267.2	264.8	244.9	217.6	210.5	287.3
Fuel max	11490.2	10865.0	10668.1	10633.8	10751.3	11049.1	10698.2
Fuel min	8499.9	9254.0	9120.9	9128.9	9487.3	9877.5	8924.6
Flight Time (s)	55.8	60.7	65.4	74.0	82.0	89.5	95.0
FT σ	3.2	2.6	2.8	2.5	2.7	2.6	2.0
FT max	63.6	67.9	75.2	81.3	91.5	97.7	101.5
FT min	38.0	51.0	56.4	65.7	73.6	82.7	88.4
Range (m)	9.1	2.5	2.6	2.6	2.5	2.5	2.5
Range σ	60.2	1.9	1.9	2.0	1.9	1.9	1.9
Range max	684.5	8.8	9.1	8.8	8.6	8.4	8.8
Range min	0.0	0.0	0.1	0.1	0.0	0.1	0.0
Speed (m/s)	8.8	8.0	8.2	8.1	8.1	8.1	8.0
Speed σ	7.4	3.6	3.5	3.5	3.5	3.5	3.6
Speed max	77.7	14.9	15.7	15.7	15.1	14.8	15.5
Speed min	0.3	0.5	0.6	0.5	0.6	0.6	0.3

Table 4.4. Performance of APDG In Atmosphere

Figure 4.35 again demonstrates the characteristic Gaussian distribution in propellant consumption, with fewer outlying low consumption runs in Case 1. Adaptive PDI (Case 7) shows a lower mean than all other cases and maintains a similar distribution as the other cases. Range, speed, and failure histograms are given in the Appendix as they are qualitatively similar to the vacuum performance figures in Section 4.0.5.

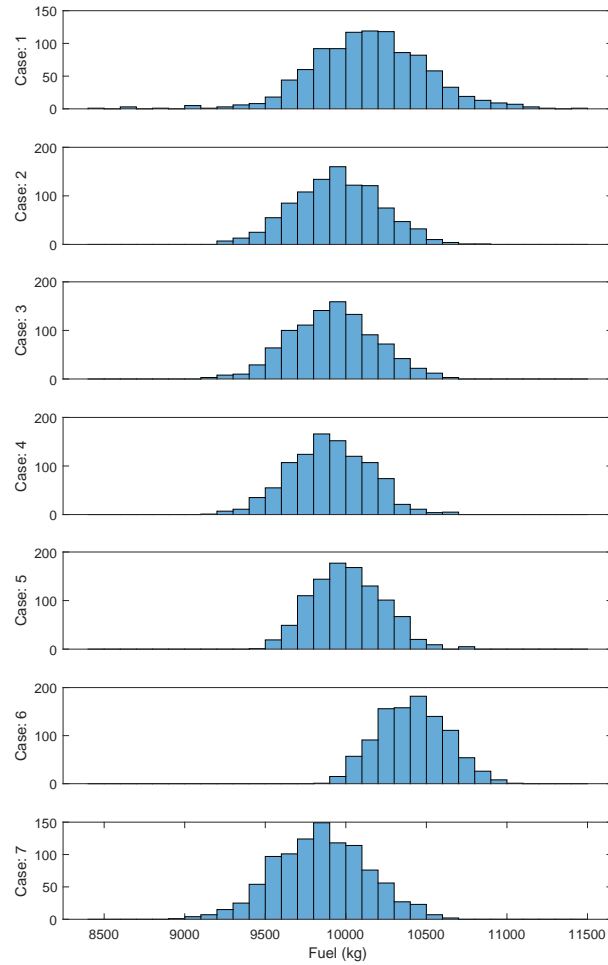


Figure 4.35. Fuel Histogram: APDG in Atmosphere

CHAPTER 5

DISCUSSION

The results in Chapter 4 have many implications on the guidance approach of APDG as well as the adaptive powered descent initiation strategy of Section 2.4. They will be discussed here, as well as the validity of the results themselves.

5.1 SIMULATION ERROR ANALYSIS

As discussed in Section 3.1, the numerical integration technique employed is a Runge-Kutta 4th order method. This method is particularly attractive in computationally expensive applications because the total accumulated error due to time integration reduces on the order $O(\Delta t^4)$ where Δt is the time integration step size, while the computational expense increases on the order $O(\Delta t)$. This means that a larger step size can produce the same order of error as an equally computationally expensive simulation using a first order scheme, saving significant computational and engineering time resources. There is a limit to the error reduction in that any finite computation produces machine error in rounding and variable storage. This simulation was run on a system with a machine error $\epsilon \approx 2 * 10^{-16}$.

To trust the validity of a simulation's results, it must be shown that the simulation is running within the numerical integration scheme's asymptotic convergence. In essence, the error should demonstrate the expected order behavior.

A 4th order scheme should show this error behavior. However, Figure 5.1 clearly shows a linear error behavior, with error reducing with order $O(\Delta t)$. Error of order $O(\Delta t)$ and $O(\Delta t^4)$ is shown for reference. This figure was generated by testing a particular moment in the simulation near the end of the trajectory without dispersion, with atmospheric effects and powered descent guidance. The baseline against which the error is measured is the a simulation result at the finest resolution, i.e. the smallest time step, $\Delta t = 2^{-13} \approx 1.2 * 10^{-4}$. Running the same test with an explicit 1st order Euler scheme produces a similar result.

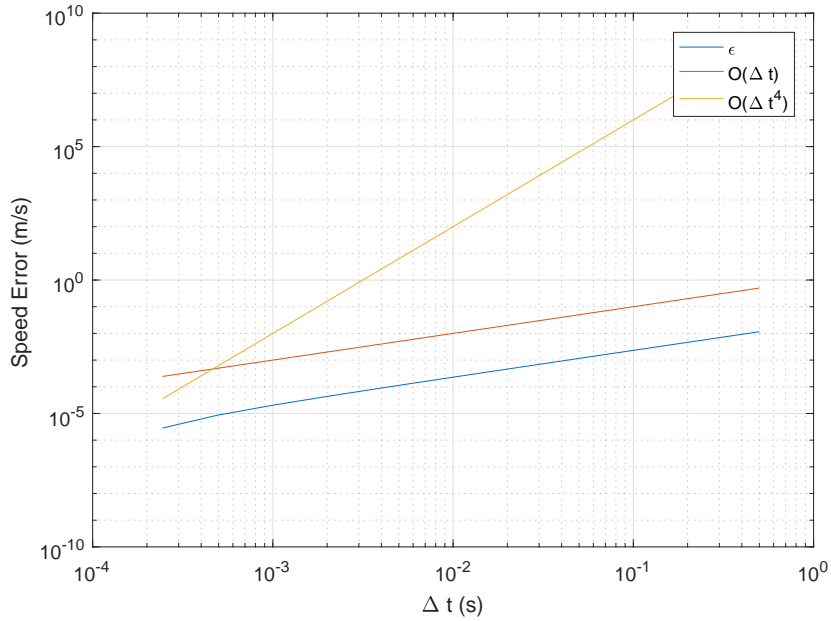


Figure 5.1. Convergence Test: Powered in Atmosphere

The reason that the error does not show $O(\Delta t^4)$ behavior is that the derivative cannot be calculated at each intermediate step required for the RK4 scheme. Specifically, the terms a_T and $\frac{F_{LD}}{m}$ representing the thrust acceleration and the aerodynamic effects in Equation (3.3) must be held constant for the intermediate derivatives. These terms are actually also functions of the state x , but they are highly non-linear. The thrust acceleration term is often actually held constant between steps since the guidance update rate is lower than the time integration rate, but every 200 time steps this assumption fails and error accumulates. Similarly, the aerodynamic model is never actually constant between time steps.

Holding terms which are functions of the state ϕ constant between time steps reduces the integration method to Explicit Euler, given in Equation (5.1).

$$\phi_{n+1} = \phi_n + \Delta t \mathbf{f}(t_n, \phi_n) \quad (5.1)$$

If these terms are removed from the simulation, representing vacuum conditions with an unpowered trajectory, the error behavior is significantly different as demonstrated

in Figure 5.2. Here we see that the magnitude of the total error is drastically lower, a factor of 10^{-7} times the atmospheric error, yet no longer decreasing with Δt . This is because all remaining error in the solution is due to machine error for any practical time step size. Testing larger time steps would lead to unrealistic guidance update rates, making the simulation invalid or impractical.

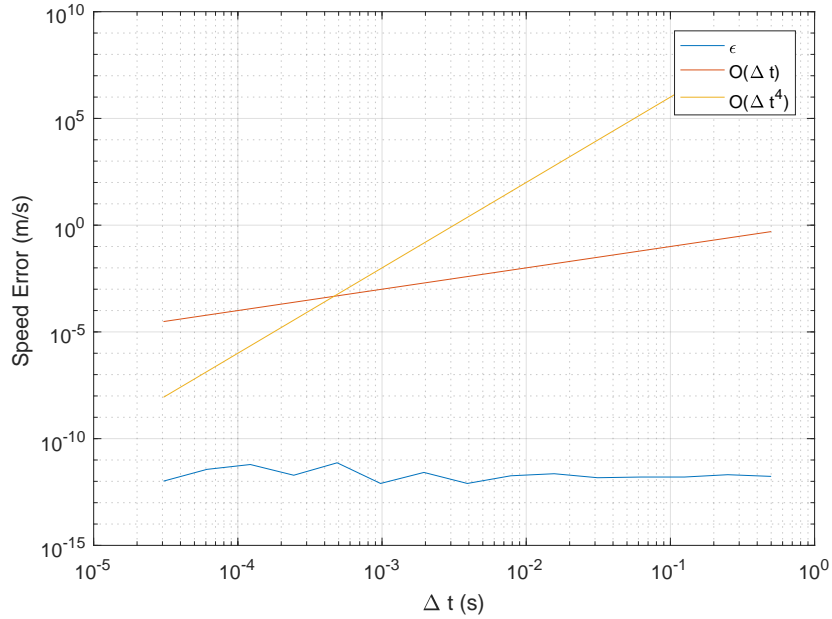


Figure 5.2. Convergence Test: Unpowered in Vacuum

However, since the simulation error is dominated by the atmospheric and thrust acceleration terms and has reached the asymptotic convergence range for these terms, the results can be taken as valid.

5.2 APOLLO POWERED DESCENT GUIDANCE

As shown in Section 2.3.3, E-Guidance minimizes the performance index in Equation (2.20). This index does not result in a fuel-optimal guidance solution, but since it is penalizing large thrust accelerations it is doing something qualitatively similar. No claim is made about the optimality of the APDG solution, but it is clear in Table 4.1 that the propellant performance is comparable. Also clear is that the guidance solution is

effective, meaning that the vehicle lands as softly and accurately under APDG as under E-Guidance. It may be slightly more sensitive to navigation error, but given quality navigation systems it can be expected to satisfy terminal constraints very accurately, as shown in Table 4.2.

The primary motivation in choice of the APDG is to ensure a practical final attitude. This aids in either landing the vehicle entirely under APDG or smoothly transitioning to a vertical descent guidance law. Figure 4.8 shows APDG's superiority to E-Guidance in this regard. APDG does a very good job of achieving nearly level vehicle orientation upon touch down. The pitch error still present is likely due almost entirely to the guidance command hold in place as described in Section 3.2, and would be easily dealt with. The significantly higher pitch error resulting from E-Guidance would have to be dealt with by another guidance phase specifically designed to ensure level landing, reducing the optimality of E-Guidance further.

5.3 ADAPTIVE POWERED DESCENT INITIATION

Section 4.0.1 shows that the criteria in Equations (2) and (3) are satisfied for the trajectories presented in Figure 3.5. It is clear that either the required thrust acceleration for a gravity turn a_{GT} must at some point in the trajectory exceed the maximum thrust acceleration provided by the vehicle a_{max} , or the trajectory must be aligned such that the downrange distance to the landing site necessarily becomes smaller than the downrange distance traveled by a gravity turn maneuver s_{GT} . Figures 4.1 and 4.2 show that one or both of these requirements are satisfied. Further, it can be shown that one of these criteria will always trigger ignition for PDI. This is because a_{GT} reflects, at minimum, the acceleration required to slow the vehicle from its current speed to the final landing speed. Since the PDI approach uses the time-to-go provided by a gravity turn maneuver, as the altitude approaches zero the time-to-go also approaches zero. With an increasing speed due to a ballistic trajectory and a decreasing time to go, a_{GT} will obviously increase until it crosses the threshold a_{max} . Similarly, if the thrust acceleration criterion is not triggered, the trajectory will necessarily overshoot the landing site. Since the downrange distance traveled is roughly proportional to the speed squared as in Equation (2.34), the range criterion will be triggered at some point before overshoot.

Confident that Adaptive PDI will trigger, the question of its performance arises. For vacuum, Table 4.3 shows PDI's propellant performance (Case 7) as middle-of-the-road compared to the other predetermined starting points. Figure 4.27 also shows that its fuel distribution is similar to the fixed initial condition cases, suggesting a similar mission risk analysis. However, without knowledge of these results, each starting point may seem as feasible as the others. Indeed, driving the initial condition closer to the landing site along the trajectory in Figure 3.5 seems ideal as the propellant requirement drops according to Table 4.3, with the minimum occurring for Case 2. But driving the ignition point too close to the landing site can result in unacceptable failure rates. Case 1 results in failures 45 out of 1000 runs, or a rate of 4.5%, wildly dangerous for a manned mission. Even in vacuum PDI provides decent fuel performance and removes the guesswork inherent in choosing predetermined ignition conditions.

In atmosphere PDI's advantage grows as evidenced by Table 4.4. Not only does Case 1 show an unacceptable manned mission failure rate of 1.3%, but PDI actually provides the best propellant performance of any Case. PDI's fuel savings come primarily from its unpowered flight. During the first 20 seconds in Figure 4.33 PDI does not burn any fuel, but it manages to reduce speed and altitude for free in Figures 4.32 and 4.30. Figure 4.20 comparing Vehicle Mass for the vacuum and atmospheric conditions using PDI shows the cumulative, increasing savings from aerodynamic effects. In thicker atmospheres, one should expect larger savings since PDI automatically takes advantage of these effects. Rather than risking failure for reduced propellant consumption, PDI ensures safety and performance.

CHAPTER 6

CONCLUSIONS AND FUTURE WORK

This chapter discusses the implications of the Adaptive PDI strategy and its wider applicability to guidance laws beyond APDG or E-Guidance. Section 6.2 recommends future study of PDI and particular avenues to explore.

6.1 ADAPTIVE POWERED DESCENT INITIATION

As discussed in Section 5.3, PDI helps provides good fuel performance as well as a safety margin in combination with APDG. However, any guidance system operating with a vehicle subject to thrust acceleration limits as in Equation (2.16) would benefit from use of the Adaptive PDI strategy. Indeed, Lu recommends this PDI strategy in cooperation with his propellant optimal guidance solution [10]. For a lower bound limit, once the engine is ignited there is an absolute minimum amount of fuel that will be consumed. PDI helps reduce that minimum by not igniting the engine until necessary. For the upper bound limit, PDI ensures that the engine is ignited in time to land safely, while predetermined ignition Cases as in Table 3.2 make no such assurances. These cases can be chosen carefully but there are inherently open-loop and cannot adjust to dispersed conditions resulting from trajectory errors or unexpected rocket parameter dispersions like reduced thrust performance in transit to the mission target planet.

PDI's closed-loop strategy which actively takes into account current vehicle conditions is invaluable for a manned mission to Mars, where there may be little opportunity to adjust mission phase plans on-line but where safety and fuel performance are of critical importance.

6.2 FUTURE WORK

The wider applicability of Adaptive PDI should be studied further. In particular, there are two major variables for implementation of PDI which depend upon proper

mission planning. These variables reflect PDI's handling of the upper and lower thrust acceleration limits as well as the strength of aerodynamic effects.

The first variable requiring further study is the time-to-go safety factor c_t as described in Section 2.3.5 which helps address the thrust acceleration magnitude upper limit as demonstrated in Figure 6.1 showing the thrust profiles of a vacuum trajectory with Adaptive PDI and APDG. With $c_t = 1.0$, the vehicle attempts a landing that requires too much thrust acceleration to achieve within the given time. This results in Figure 6.2, a plot of the speed profiles. With $c_t = 1.2$ the vehicle lands softly. This is because the time-to-go model assumes the only forces acting on the vehicle are thrust acceleration and gravitational acceleration, and plans for maximum thrust without landing site constraints, but the addition of trajectory error introduces unexpected work that needs to be done by the vehicle and the time-to-go is not large enough to allow it. Applying a safety factor accounts for the additional trajectory error and the vehicle lands softly. For the vacuum condition, a factor $c_t = 1.2$ is necessary to provide a safety margin against the modeled dispersions including the landing site trajectory error, but in atmosphere it is not necessary and $c_t = 1.0$ was sufficient since some of the momentum dissipation is provided by aerodynamic effects. Ideally, this factor would be automatically generated from mission conditions. For example, c_t could be a function of atmospheric density or some other parameter to represent the work done throughout the trajectory by aerodynamic effects.

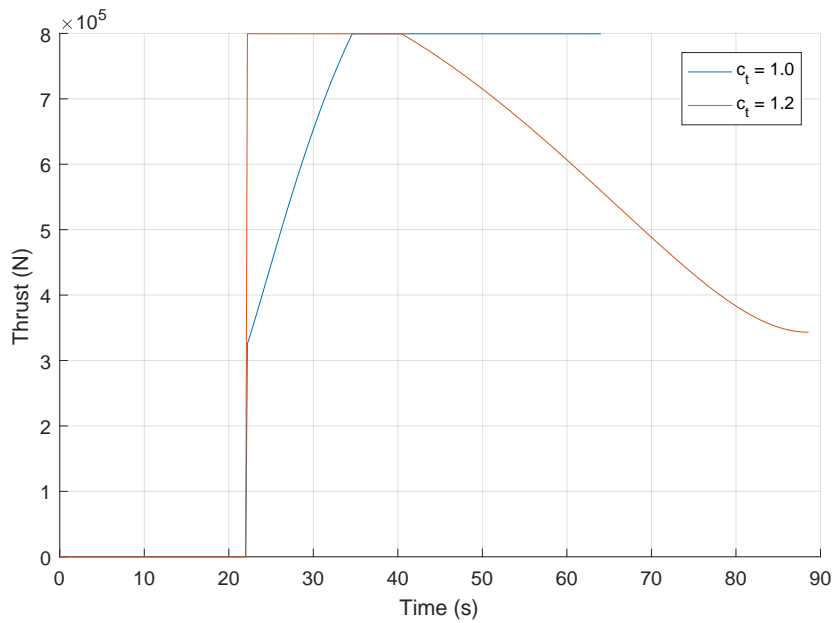


Figure 6.1. PDI Time-to-go Factor: Thrust

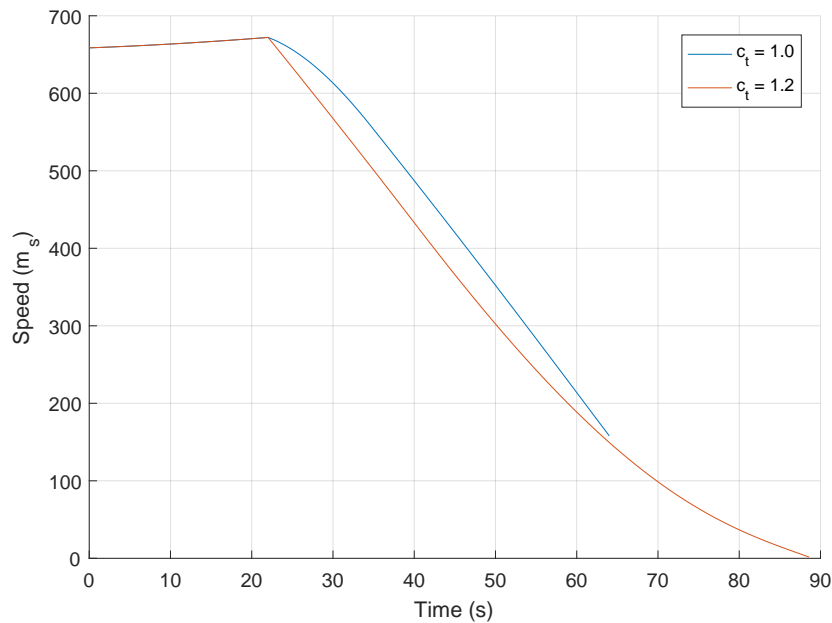


Figure 6.2. PDI Time-to-go Factor: Speed

The second variable is the threshold value or values for the thrust acceleration and downrange criteria. Here these criteria are applied directly without modifying the threshold values; the powered descent initiation is triggered when the full maximum thrust or the full downrange distance is required for a gravity turn. But these thresholds can be raised or lowered. PDI can trigger when the thrust acceleration required exceeds some fraction of the maximum thrust acceleration available, or when the downrange distance to landing site is some multiple of the downrange distance required by a gravity turn. The exact relationship between these threshold values and the time-to-go factor c_t is unknown and could be explored.

BIBLIOGRAPHY

- [1] C. CERIMELE ET AL., *A rigid mid lift-to-drag ratio approach to human mars entry, descent, and landing*, AIAA Paper, 2017-1898 (2017).
- [2] G. W. CHERRY, *A general, explicit, optimizing guidance law for rocket-propelled spaceflight*, AIAA Paper, 64-638 (1964).
- [3] C. CHOMEL, *Development of an Analytical Guidance Algorithm for Lunar Descent*, PhD thesis, The University of Texas at Austin, Austin, TX, 2007.
- [4] S. J. CITRON, S. E. DUNIN, AND H. F. MEISSINGER, *A terminal guidance technique for lunar landing*, AIAA Journal, 2 (1964), pp. 503–509.
- [5] C. S. D’SOUZA, *An optimal guidance law for planetary landing*, AIAA Paper, 97-3709 (1997).
- [6] J. H. FERZIGER AND M. PERIĆ, *Computational Methods for Fluid Dynamics*, Springer, Berlin, 2002.
- [7] H. L. JUSTH, *Mars global reference atmospheric model*. NASA, <https://see.msfc.nasa.gov/model-Marsgram>, accessed February 2018.
- [8] A. R. KLUMPP, *Apollo lunar descent guidance*, Automatica, 10 (1974), pp. 133–146.
- [9] G. LEITMANN, *Class of variational problems in rocket flight*, Journal of the Aerospace Sciences, 26 (1959), pp. 586–591.
- [10] P. LU, *Propellant-optimal powered descent guidance*, Journal of Guidance, Control, and Dynamics, (2017), pp. 1–14.
- [11] C. R. MCINNES, *Path shaping guidance for terminal lunar descent*, Acta Astronautica, 36 (1995), pp. 367–377.
- [12] J. J. MEDITCH, *On the problem of optimal thrust programming for a lunar soft landing*, IEEE Transactions on Automatic Control, 9 (1964), pp. 477–484.
- [13] T. J. MOESSER, *Guidance and navigation linear covariance analysis for lunar powered descent*, Master’s thesis, Utah State University, Logan, UT, 2010.
- [14] F. NAJSON AND K. D. MEASE, *Computationally inexpensive guidance algorithm for fuel-efficient terminal descent*, Journal of Guidance, Control, and Dynamics, 29 (2006), pp. 955–964.

- [15] S. R. PLOEN, A. B. ACIKMESE, AND A. WOLF, *A comparison of powered descent guidance laws for mars pinpoint landing*, AIAA, 2006-6676 (2006).
- [16] J. R. REA AND R. H. BISHOP, *Analytical dimensional reduction of a fuel optimal powered descent subproblem*, AIAA Paper, 2010-8026 (2010).
- [17] I. M. ROSS, *How to find minimum-fuel controllers*, AIAA, 2004-5346 (2004).
- [18] R. R. SOSTARIC AND J. R. REA, *Powered descent guidance methods for the moon and mars*, AIAA, 2005-6287 (2005).

APPENDIX
DISPERSED TRAJECTORY FIGURES

DISPERSED TRAJECTORY FIGURES

Given here are histograms showing the distribution of various performance variables relating to the vacuum and atmospheric conditions for a powered landing and descent under APDG as described in Chapters 3 and 4.

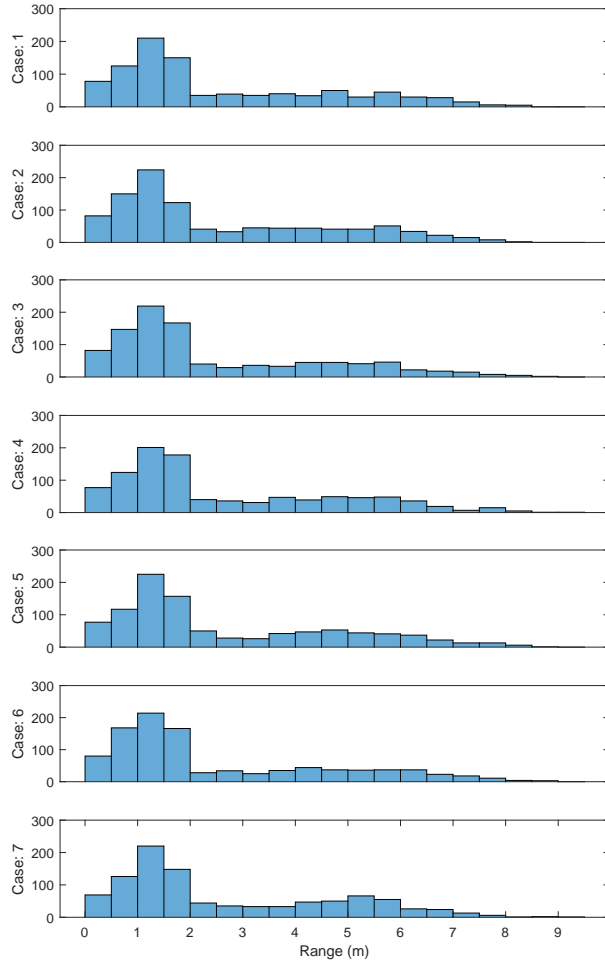


Figure A.1. Ground Range Histogram: APDG in Vacuum

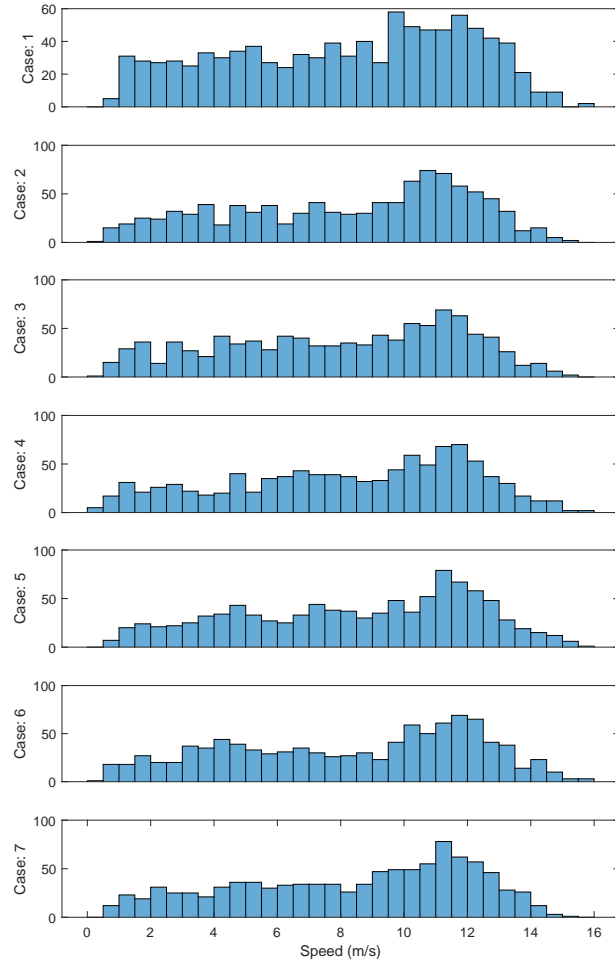


Figure A.2. Speed Histogram: APDG in Vacuum

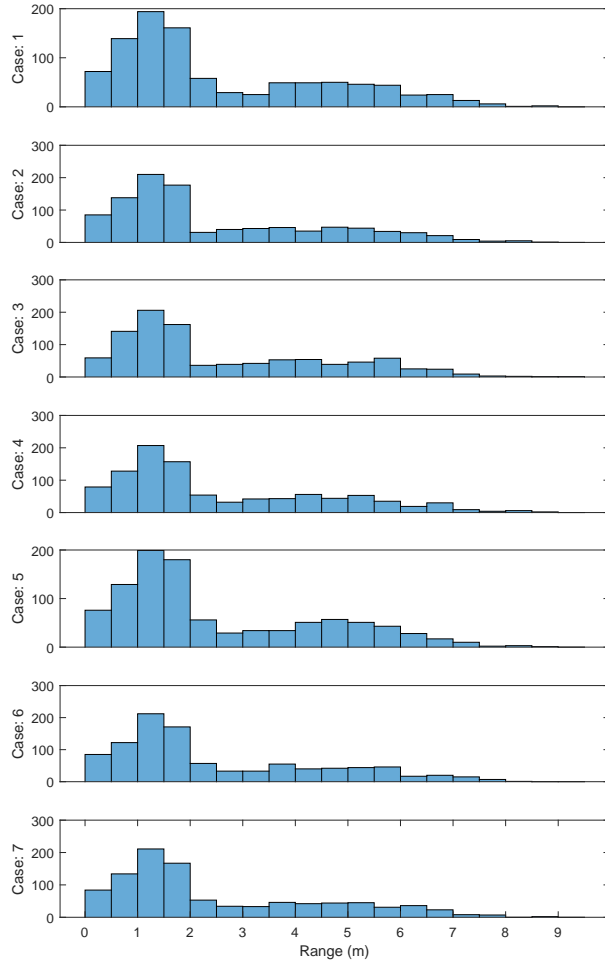


Figure A.3. Ground Range Histogram: APDG in Atmosphere

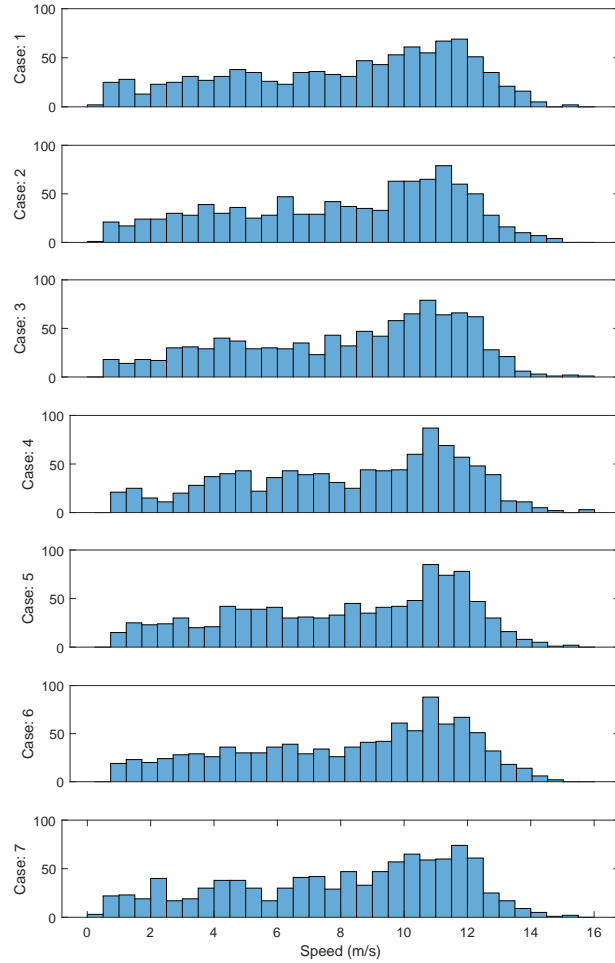


Figure A.4. Speed Histogram: APDG in Atmosphere

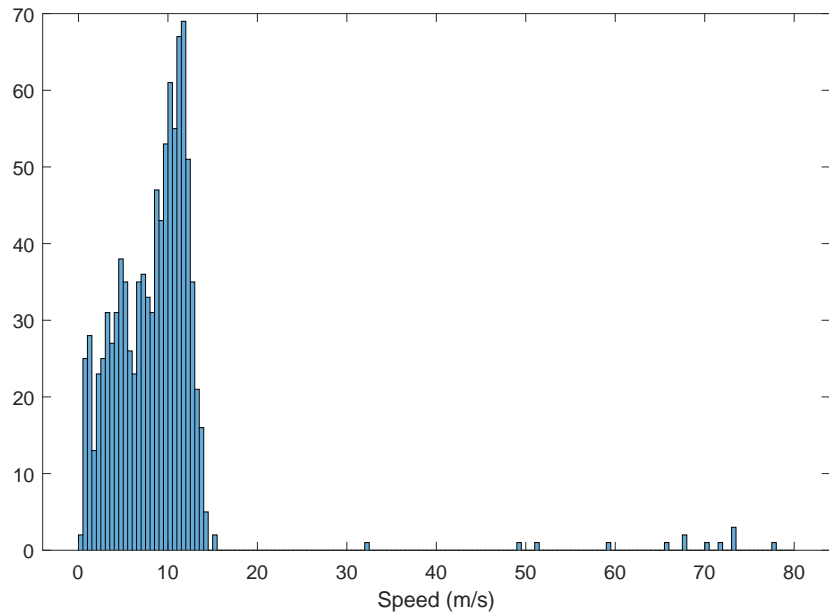


Figure A.5. Failures Histogram: APDG in Atmosphere